CHAPTER III

RESULTS AND DISCUSSION

3.1 Effect of Molecular Weight

In this study we used three LLDPE's of different molecular weights according to a tabulation below

LLDPE	M_W (g/mol)	M_W/M_n
L1810F	$1.27x10^5$	9.23
L2009F	$1.03x10^5$	8.47
L2020F	$6.07x10^4$	6.01

3.1.1 Flow Curves

Flow curve is the plot of the wall shear stress (τ_w) versus the apparent strain rate ($\dot{\gamma}_a$) obtained by a capillary rheometer. Features of the flow curve are often associated with other observations such as extrudate distortion, fluctuation in load and flow rate. We found at least five regimes, according to the type of the flow behaviour and the appearances of the extrudate surfaces. The three flow curves for the smaller capillary, l_c = 22.5 mm and d_c = 0.7645 mm (die no. 614) , are shown in figures 3.1 (a), (b) and (c). In figure 3.1 (a), there are five distinct regimes in the flow curve. The regime I, which occured below the first critical wall shear stress (τ_w) of $3.25x10^5$ N/m^2, was a stable flow regime, and the extrudate produced has a smooth surface. The regime II was observed for the shear stresses in the range of $3.25x10^5$ - $3.67x10^5$ N/m^2. Although the flows in the regime I and the regime II were steady, but

the regime II can be separated from the regime I by the appearance of a sharkskin surface, which has skin roughness with high frequency but with some order [figure 3.2 (b)]. The onset of the sharkskin was indicated by a distinct change in the slope of the flow curve at the first critical wall shear stress. The regime III was an oscillating flow regime. Here, the stress became double valued, and the extrudate alternated in periodic fashion between a sharkskin and a smooth surface section. Here the polymer chains were disentangled periodically from each other and the slip occured at the polymer/metal interface, resulting in two unstable velocity profiles at the same plunger speed (or apparent strain rate). In the regime IV, as the stress increased, the chains were still disentangled but the die was too short to have the time for the chain relaxation so the flow appeared steady. The extrudate was smooth. At the higher strain rates, we observed the melt fracture whose surface had a more severity and less order than the sharkskin surface. In regime IV we devided it into two regimes (IV-a and IV-b) depending on whether the extrudate was smooth or a melt fracture. In the regime V, when the wall shear stress was increased as high as the value of the onset of the regime III, the oscillating flow occured again. The extrudate was melt fracture for both the upper branch and the lower branch.

Table 3. 1 The flow behaviour and the extrudate surface in each regime of the three different M_W

Regime	Flow Behaviour	Extrudate Surface
I	steady flow	smooth
II	steady flow	sharkskin
III	oscillatory flow	smooth and sharkskin
IV-a	steady flow	smooth
IV-b	steady flow	melt fracture
V	oscillatory flow	melt fracture

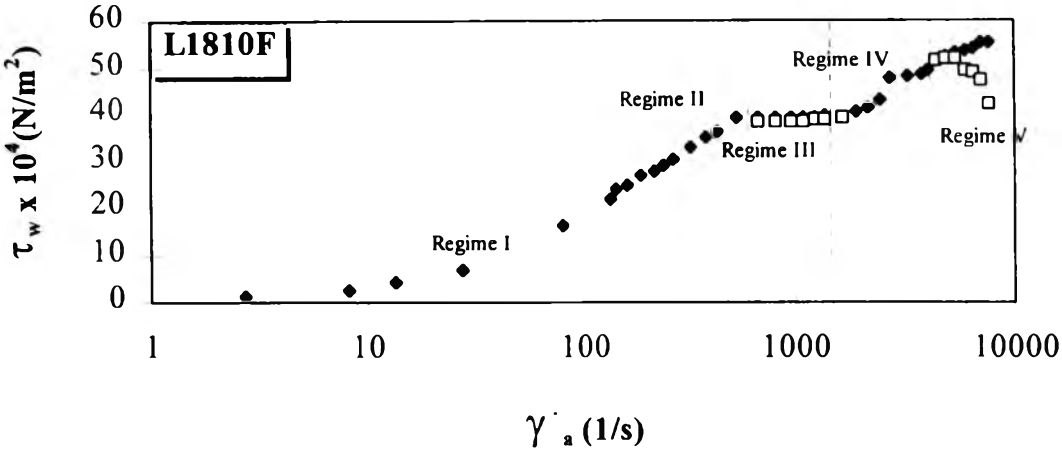

Figure 3.1(a) Flow curves of LLDPE (M_W=1.27x10^5) at 185°C.

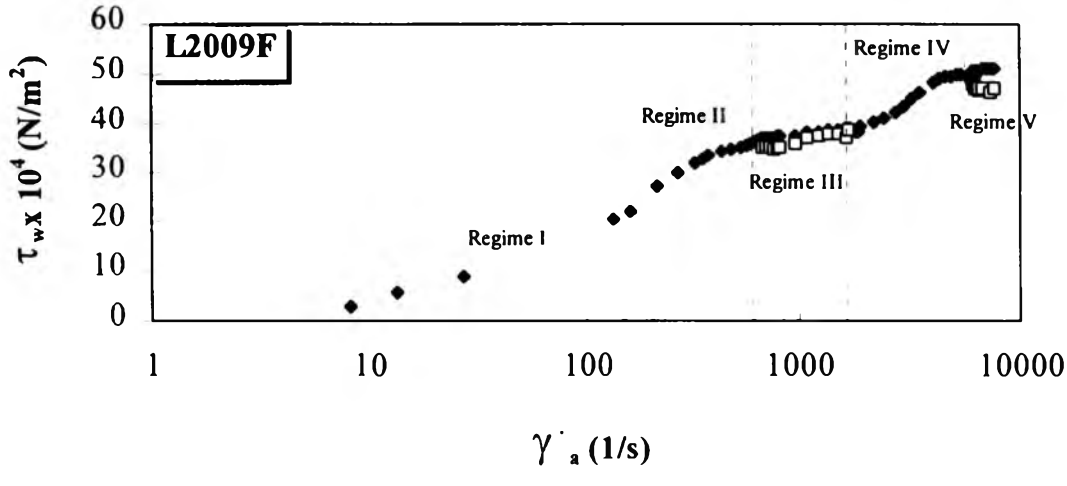

Figure 3.1(b) Flow curves of LLDPE (M_W=1.03x10^5) at 185°C.

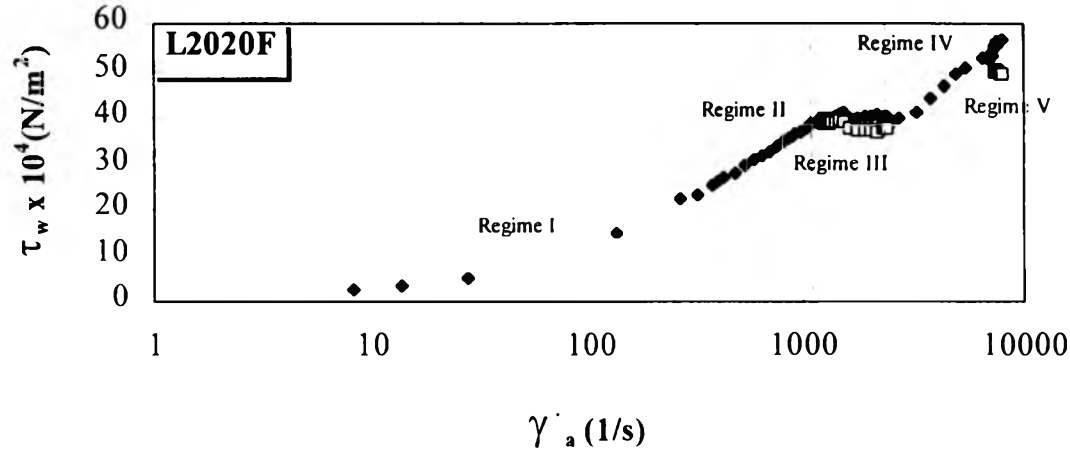

Figure 3.1(c) Flow curves of LLDPE (M_W=6.07x10^4) at 185°C.

3.1.2 Critical Values

The conditions for the transitions of the various regimes for the three LLDPE's different molecular weights used in this work are summarized in the Table 3.2 below.

Table 3. 2 The critical wall stresses and strain rates of the three LLDPE's of different M_W

Regime	Critical Data	**L1810F**	**L2009F**	**L2020F**
II	$\dot{\gamma}_{a,c}$ (1/s)	328	352	758
	$\tau_{w,c}$ (N/m^2)	3.25E+05	3.29E+05	3.40E+05
III	$\dot{\gamma}_{a,c}$ (1/s)	531	650	1220
	$\tau_{w,c}$ (N/m^2)	3.67E+05	3.68E+05	3.87E+05
IV-a	$\dot{\gamma}_{a,c}$ (1/s)	1710	1730	2400
	$\tau_{w,c}$ (N/m^2)	3.80E+05	3.89E+05	3.92E+05
IV-b	$\dot{\gamma}_{a,c}$ (1/s)	2710	2710	3790
	$\tau_{w,c}$ (N/m^2)	4.47E+05	4.24E+05	4.42E+05
V	$\dot{\gamma}_{a,c}$ (1/s)	5390	6060	7170
	$\tau_{w,c}$ (N/m^2)	4.96E+05	5.04E+05	5.32E+05

It can be seen from this regime that the critical wall shear stress for each regime is independent of molecular weight. However, the critical wall shear stress depends on the regime or the skin texture that appears; $\tau_{W,C}$ is larger for regime IV-a than regime III, for an example. Therefore, an appearance of each skin texture requires a different level of stress to initiate a surface modification. On the other hand, we can see that for each regime the critical strain rate depends on molecular weight. The critical strain rate is higher for an LLDPE with a lower molecular weight. This is simply because the LLDPE with a lower molecular weight has a lower viscosity, therefore the critical strain rate has to be higher if the critical wall shear stress is to be the same.

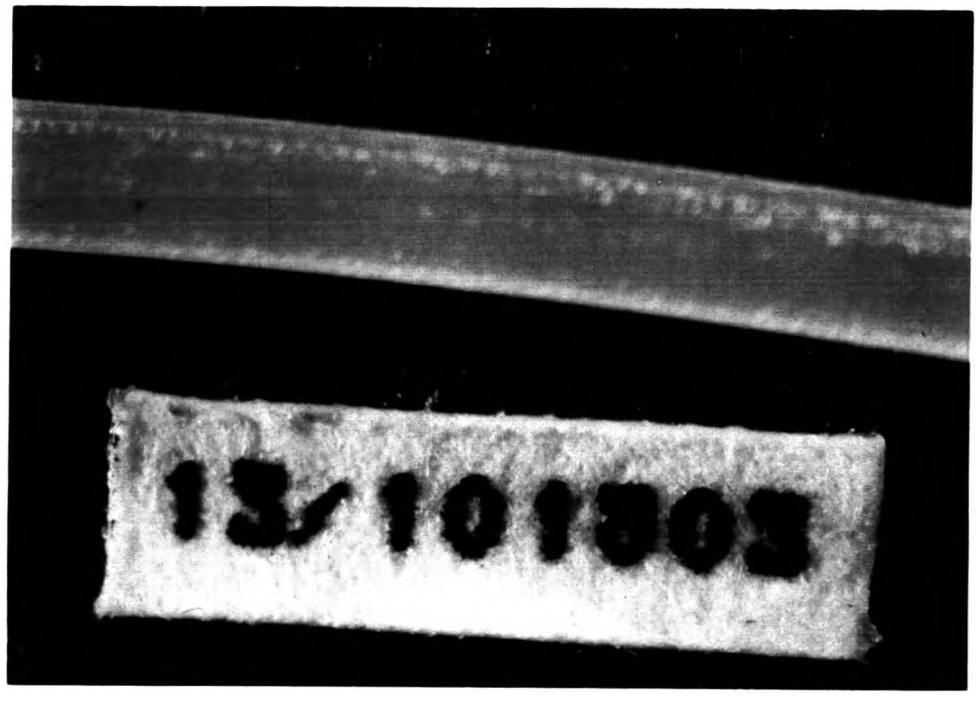

(a-1) 20x magnification

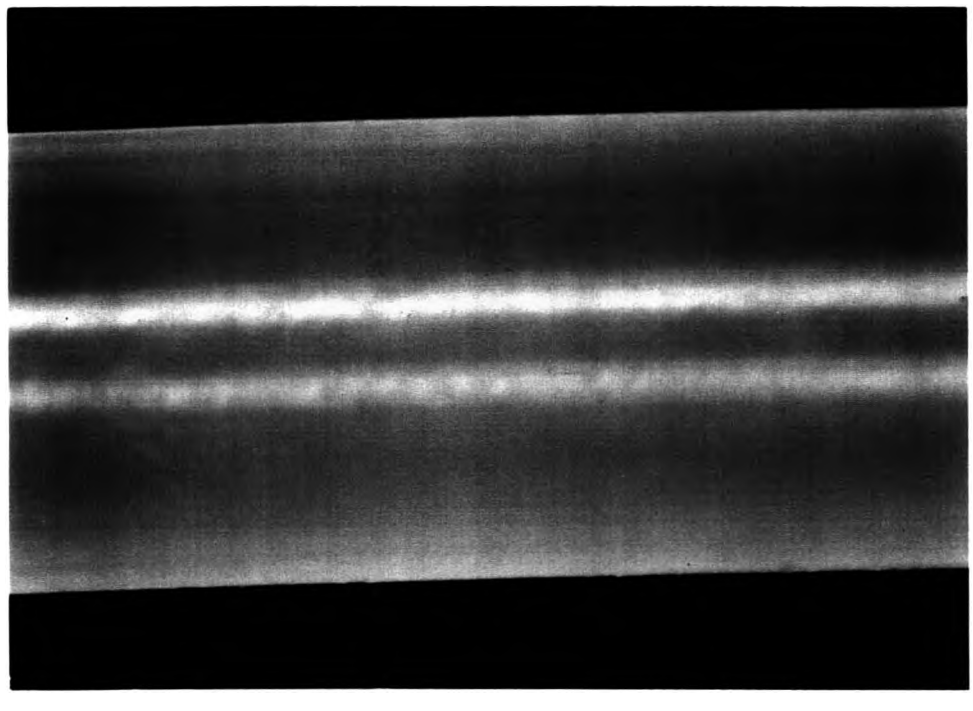

(a-2) 100x magnification

Figure 3. 2 (a) LLDPE (L1810F) extrudate displaying a smooth surface in regime I.

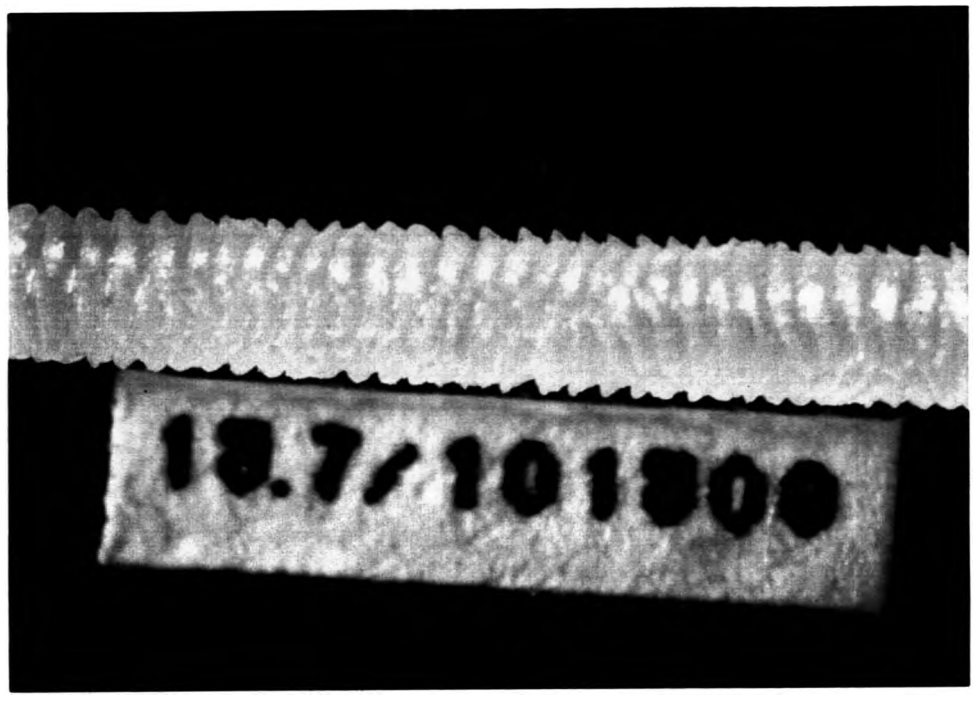

(b-1) 20x magnification

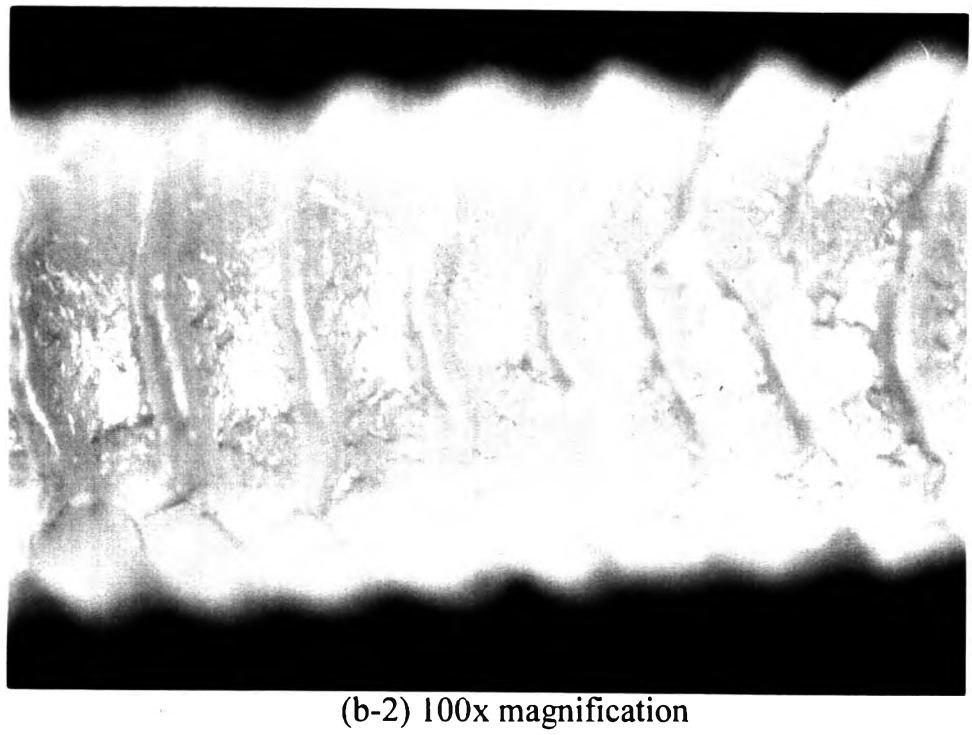

(b-2) 100x magnification

Figure 3.2 (b) LLDPE (L1810F) extrudate displaying a sharkskin surface in regime II.

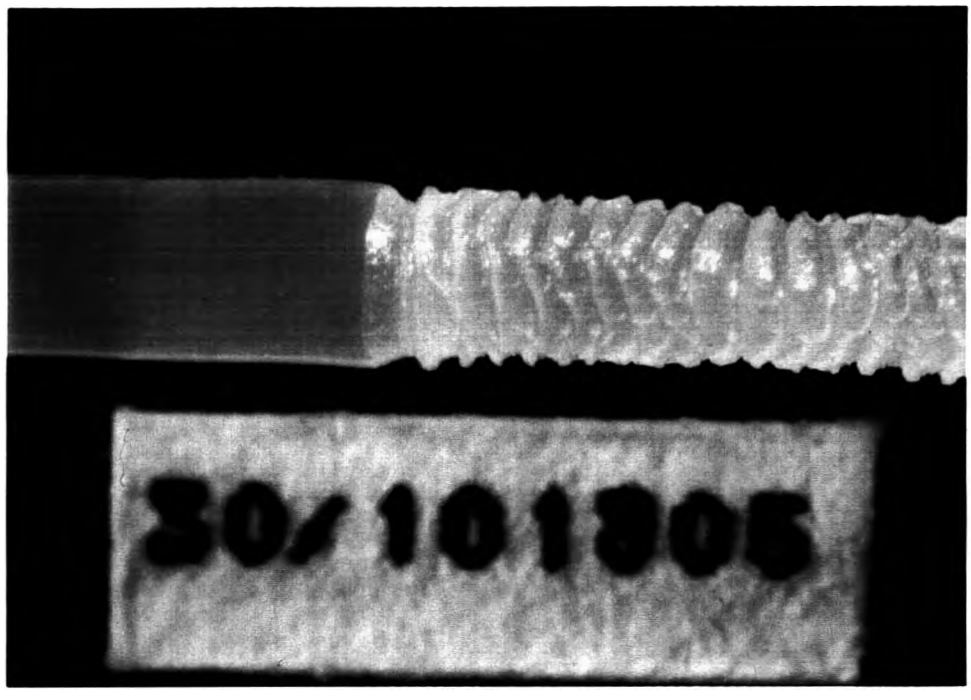

(c-1) 20x magnification

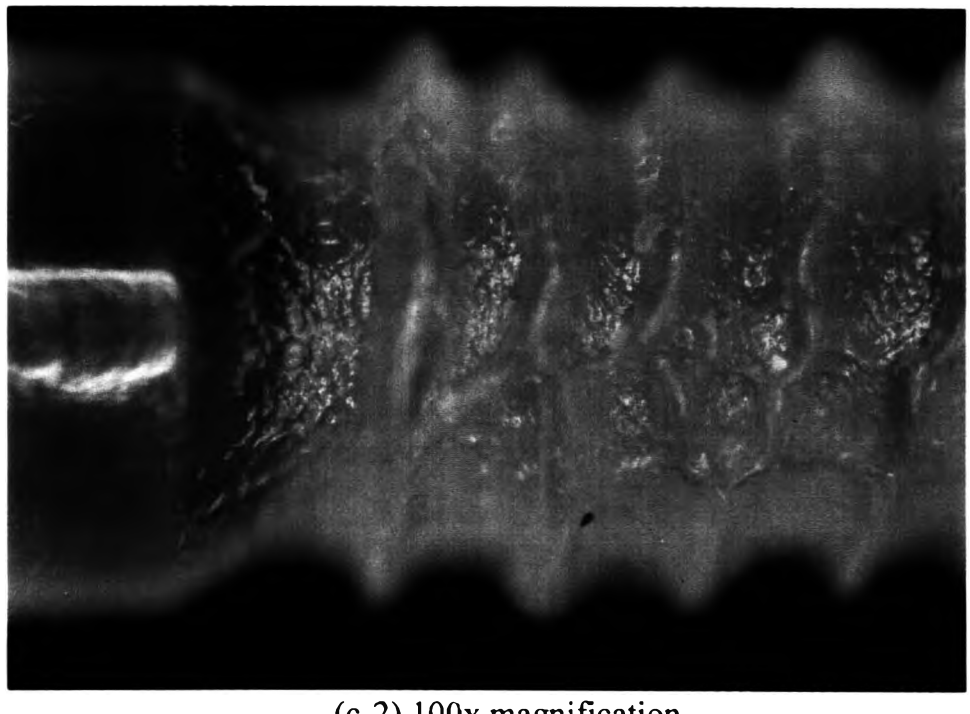

(c-2) 100x magnification

Figure 3.2 (c) LLDPE (L1810F) extrudate displaying alternating surfaces between a sharkskin and a smooth surface in regime III.

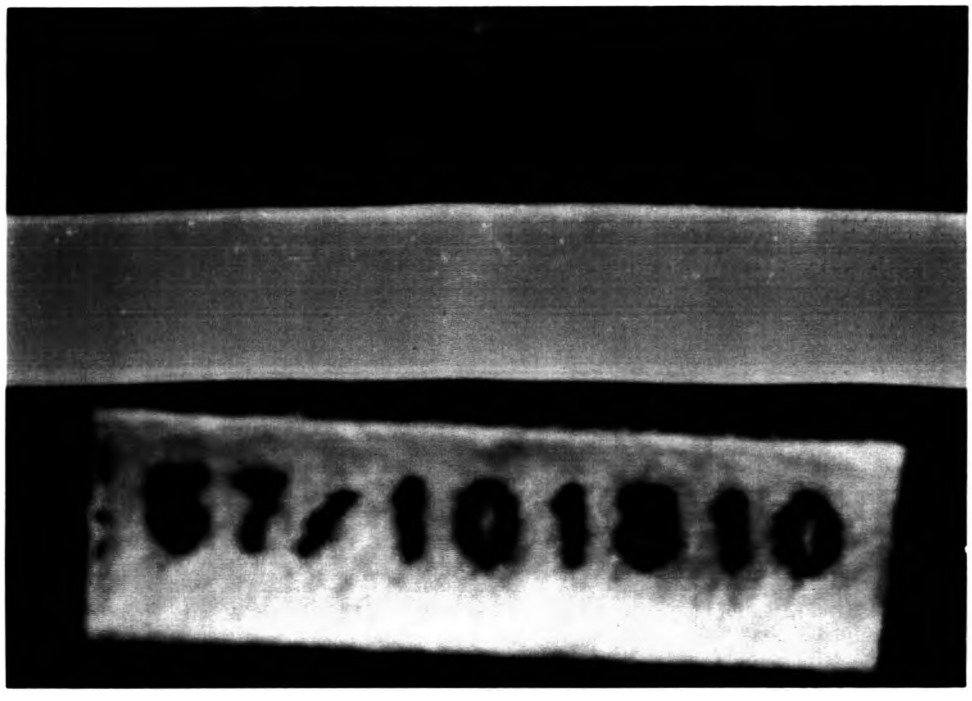

(d-1) 20x magnification

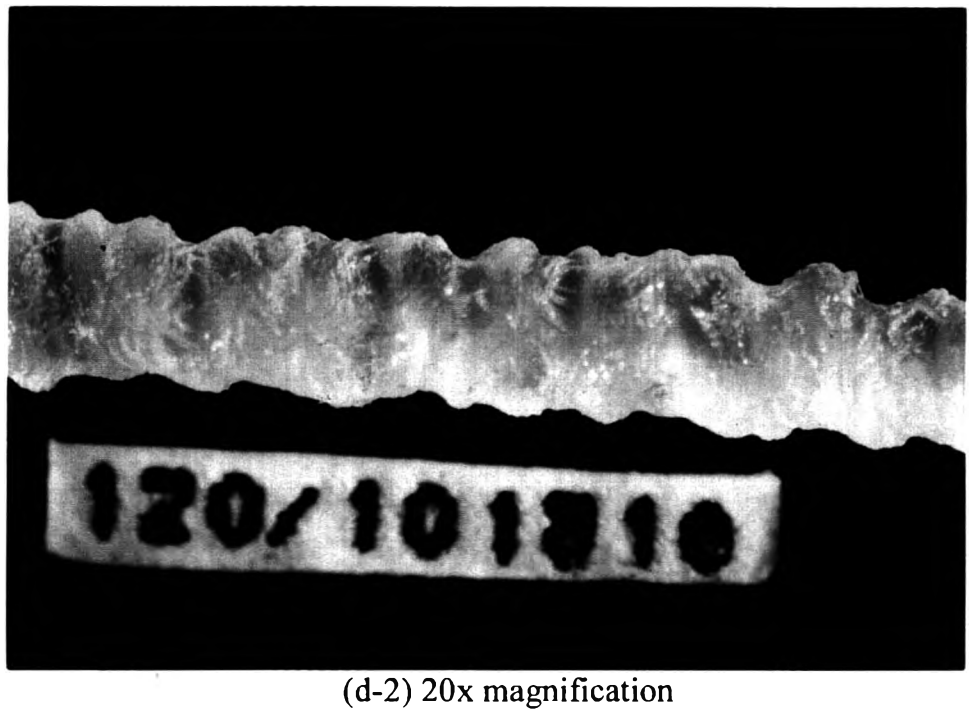

(d-2) 20x magnification

Figure 3.2 (d) LLDPE (L1810F) extrudate displaying (d-1) smooth surface and (d-2) melt fracture surface in regime IV-a and regime IV-b respectively .

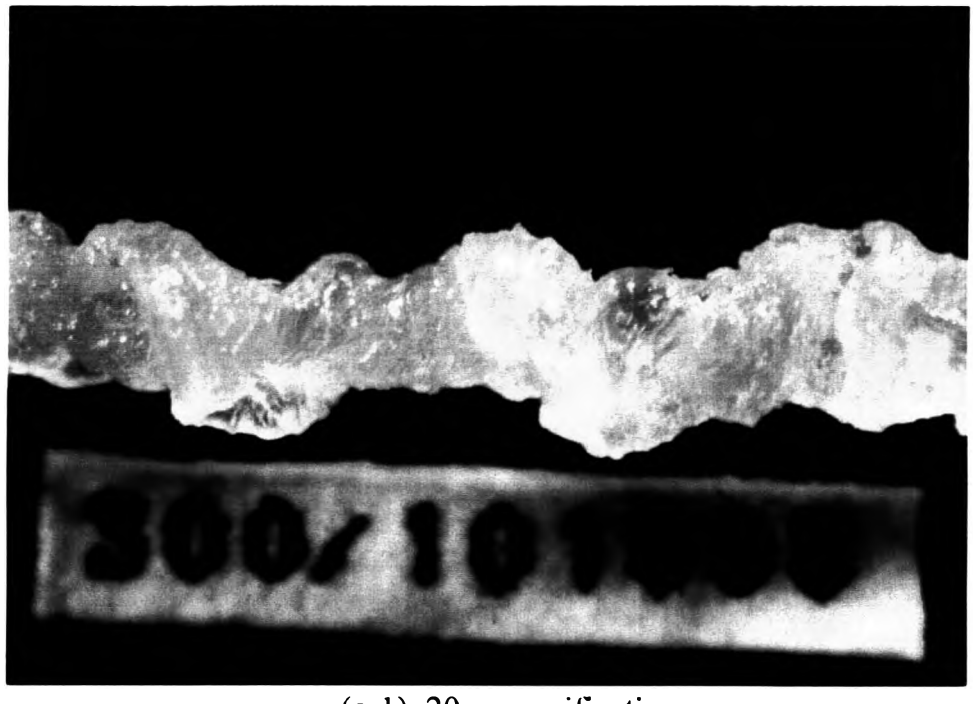

(e-1) 20x magnification

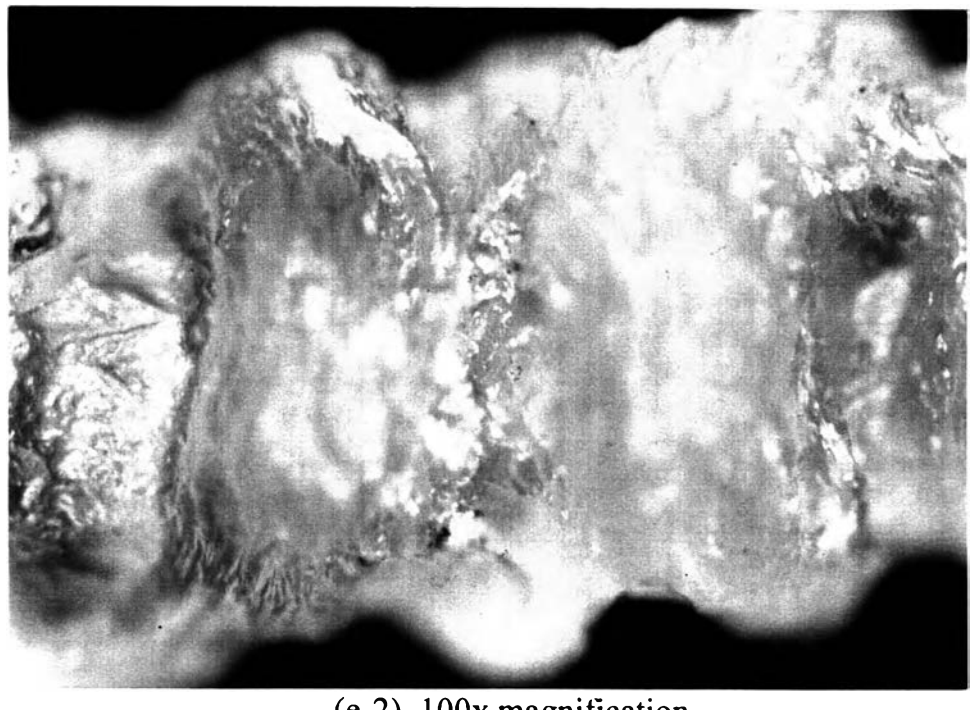

(e-2) 100x magnification

Figure 3.2 (e) LLDPE (L1810F) extrudate displaying a melt fracture surface in regimeV.

3.1.3 Surface Textures

The three LLDPE's of different molecular weights produce similar surface textures for each regime. The photographs of the skin textures are shown in figures 3.2(a)-(e).

Figures 3.2 a-1 and a-2 show a smooth skin extrudate of regime I. At the 20x magnification, we notice that the skin texture is smooth, but at 100x magnification, the picture reveals that the skin has a shiny appearance. Therefore, we can call this skin texture a glossy smooth skin, to be differentiated from a hazy smooth skin.

Figures 3.2 b-1 and b-2 show a sharkskin extrudate of regime II. The sharkskin of figure 3.2 b-1 has a similar appearance to those of the sharkskins found in previous published literature (Kalika and Denn, 1987). Upon increasing to 100x magnification, we can see from figure 3.2 b-1 that beneath and between the sharkskin ripples, the skin surface has some small but random roughness.

Figures 3.2 c-1 and c-2 show an alternating sharkskin/smooth extrudate. The smooth segment is the same as the extrudate found in regime I. The sharkskin segment is the same as that in regime II.

Figures 3.2 d-1 and d-2 show a smooth skin and a melt fracture in regime IV-a and regime IV-b respectively. The extrudate in figure 3.2 d-1 is a glossy smooth skin. In regime IV-b d-2, we see that the melt fracture has a random surface variations with amplitudes comparable to the capillary size (above 20 %). Our identification of the melt fracture is the same as other previous investigators who sometimes employed the name wavy fracture.

Figures 3.2 e-1 and e-2 show a melt fracture extrudate in regime V. We notice here that the surface distortions are very severe. The magnitude of random variations in the extrudate cross section is comparable to the capillary diameter. Closer examination at 100 x magnification reveals that beneath the

large amplitude variations, there are some surface disorders of small amplitudes.

3.2 Effect of Die Geometry

In this study we used the two capillary dies which have nearly the same l_c/d_c :

No.614 ; l_c = 22.5 mm, d_c = 0.7645 mm, l_c/d_c = 33.4 and

No1855 ; l_c = 50.9 mm, d_c = 1.2751 mm, l_c/d_c = 39.9.

3.2.1 Flow Curves

The flow curve for the larger capillary, l_c = 50.9 mm. and d_c = 1.2751 mm.(die no.1855) is shown in figure 3. 3 (b). There are four distinct regimes of flow. The regime I was a stable flow regime, where the extrudate had a smooth surface. The regime II, which was observed at the wall shear stress of 3.85x105 N/m^2, was identified by a sharkskin surface. The regime III was an oscillating regime; the extrudate alternated in a periodic fashion between a sharkskin and a smooth surface. The load fluctuation deminished at the beginning of the regime IV. Although the extrudate in each regime was the same as the extrudate surface from the smaller capillary die, regime V of the larger capillary die disappeared. This was because of the limitation of the plunger velocity of the Instron machine; it could not produce the higher strain rate needed to reach the critical shear stress for the oscillation to reoccur.

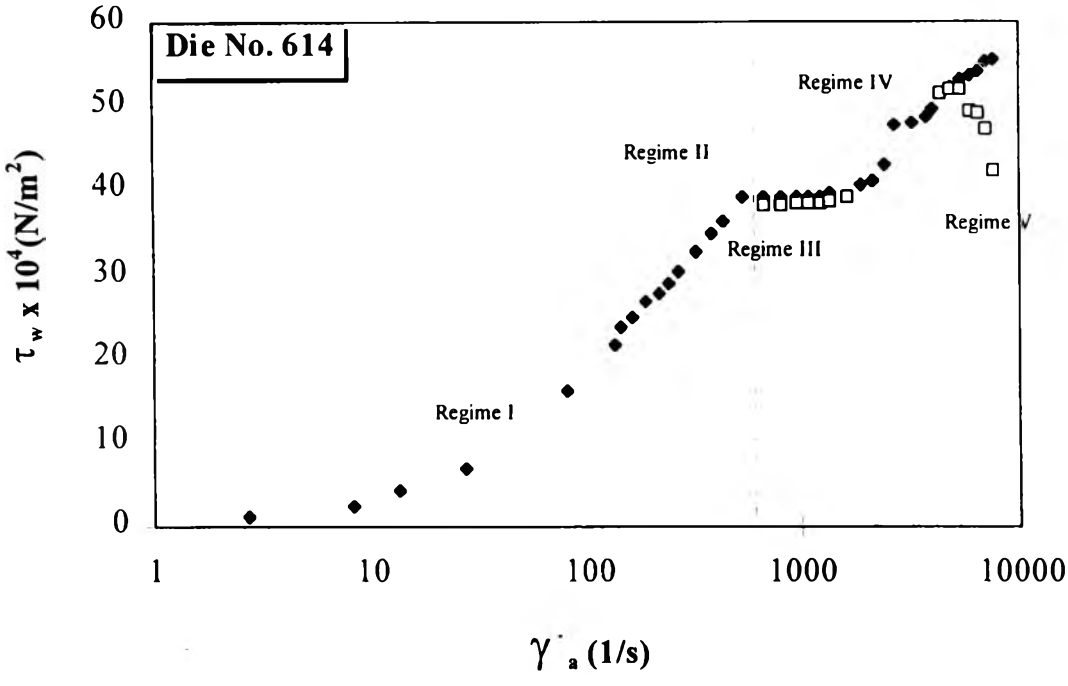

Figure 3.3(a) Flow curves of LLDPE (L1810F) of the die No.614 (l_c = 22.5 mm, d_c = 0.7645 mm) at 185°C.

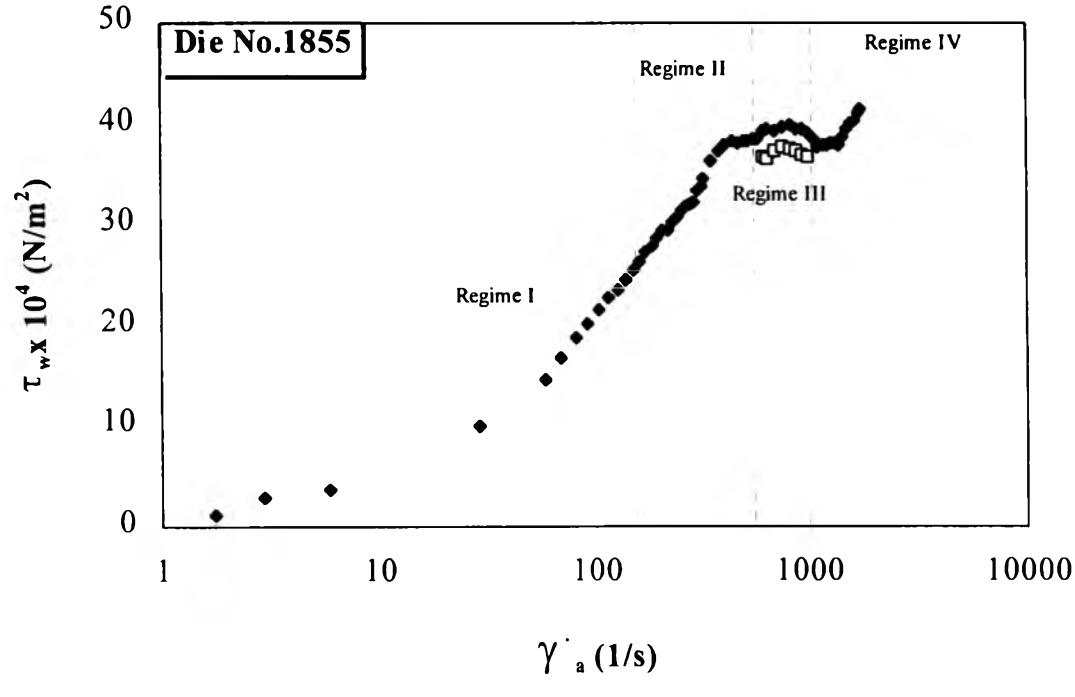

Figure 3.3(b) Flow curves of LLDPE (L1810F) of the die No1855 (l_c = 50.9 mm, d_c = 1.2751 mm) at 185°C.

Table 3. 3 The flow behaviour and the extrudate surface in each regime of the two different capillary dies for LLDPE (L1810F)

Regime	Flow Behaviour	d_c = 0.7645 mm	d_c = 1.2751 mm
I	steady flow	smooth	smooth
II	steady flow	sharkskin	sharkskin
III	oscillatory flow	smooth /sharkskin	smooth /sharkskin
IV-a	steady flow	smooth	smooth
IV-b	steady flow	melt fracture	melt fracture
V	oscillatory flow	melt fracture	-

Table 3. 4 The critical wall stresses and strain rates of two different capillary dies of LLDPE (L1810F)

Regime	Critical Data	d_c = 0.7645 mm	d_c = 1.2751 mm
II	$\dot{\gamma}_{a,c}$ (1/s)	328	292
	$\tau_{w,c}$ (N/m^2)	3.25E+05	3.23E+05
III	$\dot{\gamma}_{a,c}$ (1/s)	531	584
	$\tau_{w,c}$ (N/m^2)	3.67E+05	3.85E+05
IV-a	$\dot{\gamma}_{a,c}$ (1/s)	1710	1050
	$\tau_{w,c}$ (N/m^2)	3.80E+05	3.86E+05
IV-b	$\dot{\gamma}_{a,c}$ (1/s)	2710	1460
	$\tau_{w,c}$ (N/m^2)	4.47E+05	3.87E+05
V	$\dot{\gamma}_{a,c}$ (1/s)	5390	-
	$\tau_{w,c}$ (N/m^2)	4.96E+05	-

3.2.2 Critical Values

The conditions for the transitions among the various regimes for the two capillary diameters used in this work are summarized in Table 3.4. Eventhough the diameter and length are different but the capillaries used have

nearly the same length-to-diameter (L/D) ratios. The critical wall shear stress is independent of the die geometry but the strain rate depends on the die geometry. This is possibly the effect of viscosity of the polymer melt, a difference in melt compressibilty and possibly a difference in the upstream condition.

3.3 Slip Velocity

3.3.1 Bifurcation Diagrams

The description of the forced and parametric oscillators allows us to tackle another idea which is basic to study of dynamical systems: namely bifurcation (Berge, 1984). In the oscillating regimes, the stress becomes double valued at a fixed strain rate. In figure 3.4, the onset point of the regime III is different from the onset of the regime V. In figure 3.4 (a); the bifurcation diagram of the regime III is a *subcritical* bifurcation; it shows an abrupt transition at the onset, moreover it has different onset points when the experiment plunger velocity was reversed. This phenomenon is called *hysteresis.* In this regime the terminal point is also a subcritical for the same reason. The extrudate surface was alternated between the sharkskin surface that appeared at the upper branch and the smooth surface that appeared at the lower branch of the flow curve. Figure 3. 4 (b) shows the onset of the regime V, the bifurcation diagram is a *supercritical* bifurcation because the onset is smooth and independent of hysteresis. The melt fracture surfaces which appeared on the upper and the lower branches of the flow curve had no visible difference in appearance.

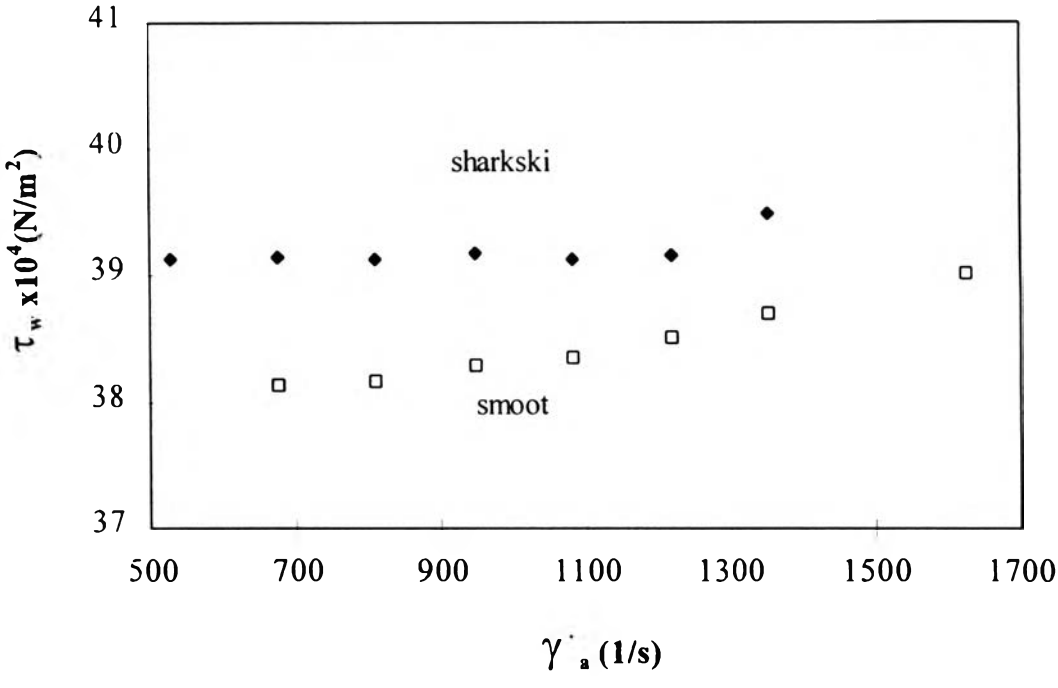

Figure 3.4(a) The wall shear stress vs. the apparent strain rate of LLDPE (L1810F) shows a subcritical bifurcation diagram in regimes III.

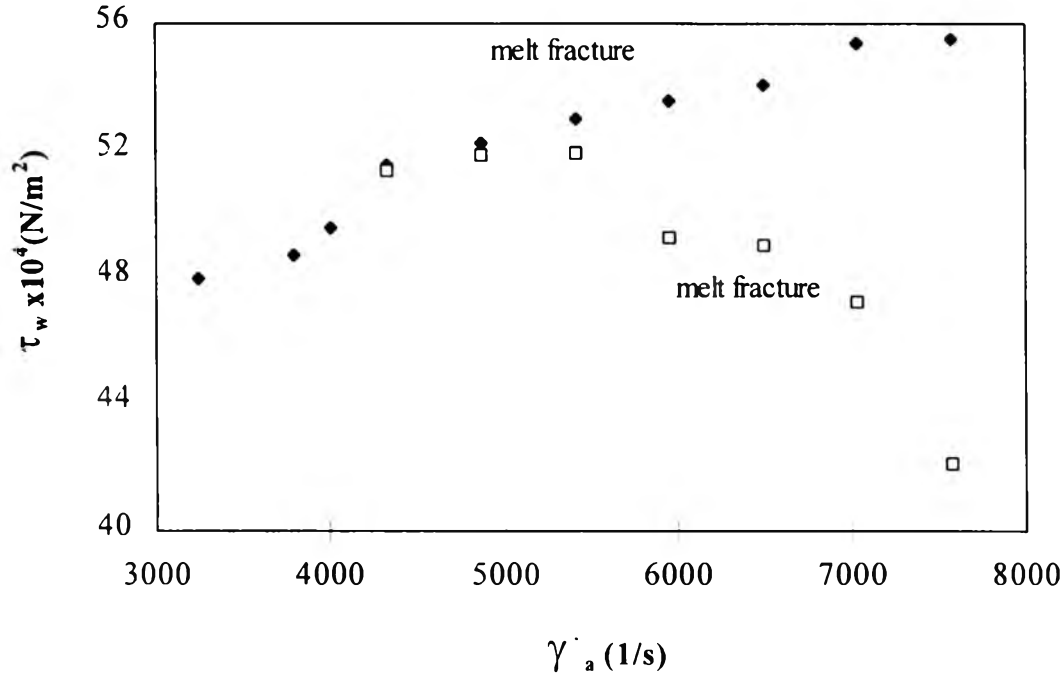

Figure 3.4(b) The wall shear stress vs. the apparent strain rate of LLDPE (L1810F) shows a supercritical bifurcation diagram in regimes III.

3.3.2 Slip Velocity (V_S)

The slip velocities in oscillating regimes was calculated from the equation 2.18. and plotted in figure 3.5 as a function of the apparent strain rate. The slip velocity seems to increase linearly with the apparent strain rate in regime III but increase nonlinearly in regime V. The slip velocity occurs from the interaction between the polymer melt and the metal surface (Ramamurthy, 1986) and can be obtained from the oscillating regimes using the periodic load fluctuations when the rheometer was operated in the constant plunger velocity mode. The extrudate produced during oscillation cycle consisted of two distinct surfaces: a sharkskin section with maximum stress, and smooth section with minimum stress. Kalika and Denn (1987) has identified the smooth, glossy section extrudate with the decreasing part of pressure cycle. This identification is consistent with our observations. The sharkskin section in the oscillating regime has the same appearance as sharkskin surface in the second regime.

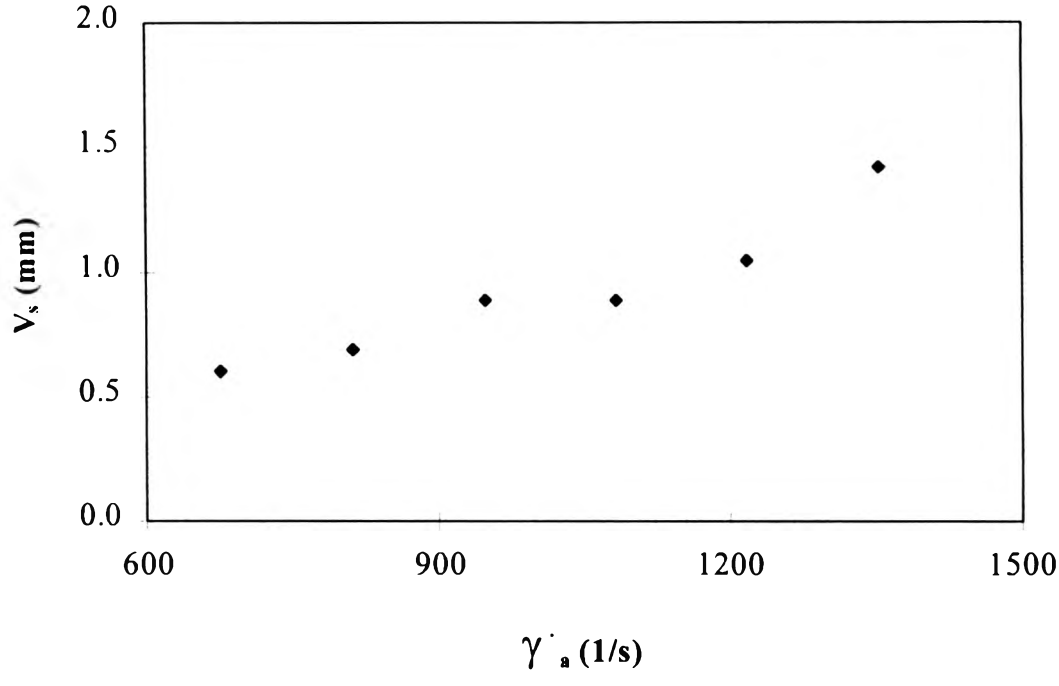

Figure 3. 5(a) Slip velocity as a function of strain rate of LLDPE (L1810F) in regime III.

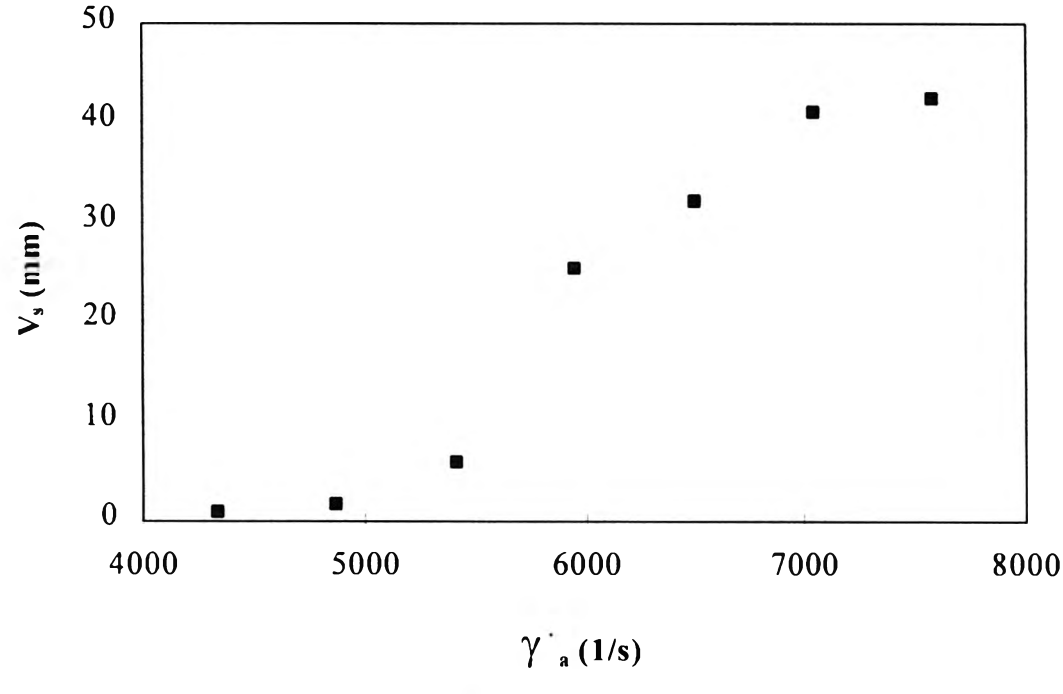

Figure 3. 5(b) Slip velocity as a function of strain rate of LLDPE (L1810F) in regime V.

3.3.3 Hopf Bifurcation

A transition from a steady state to a limit cycle or periodicity is called a *Hopf bifurcation* (Berge, 1984). Generally, a Hopf bifurcation has two common properties associated; a property of a system is proportional to $|\varepsilon-\varepsilon_c|^{1/2}$ where ε and ε_c are a bifurcation parameter and its critical value respectively. The second property associated with a Hopf bifurcation is namely the wavelength or the period is independent of $|\varepsilon-\varepsilon_c|^{1/2}$. In our capillary melt flow, we found that V_S is indeed proportional to $|\dot{\gamma}_a - \dot{\gamma}_{a,c}|^{1/2}$ as shown in figures 3.6(a)-(b). Therefore, the regime III corresponds to a subcritical Hopf bifurcation and regime V corresponds to a supercritical Hopf bifurcation. In table 3.5 we show the slope of V_S vs.$|\dot{\gamma}_a - \dot{\gamma}_{a,c}|^{1/2}$. In the regime V, the magnitude of the slope is inversely proportional to the molecular weight.

Table 3.5 The slope of V_S vs. $|\dot{\gamma}_a - \dot{\gamma}_{a,c}|^{1/2}$ of the three LLDPE's of different molecular weights

Materials	slope of V_S vs. $\|\dot{\gamma}_a - \dot{\gamma}_{a,c}\|^{1/2}$ Regime III	slope of V_S vs. $\|\dot{\gamma}_a - \dot{\gamma}_{a,c}\|^{1/2}$ Regime V
L1810F	0.0821	0.1497
L2009F	0.1303	0.9458
L2020F	0.1198	2.389

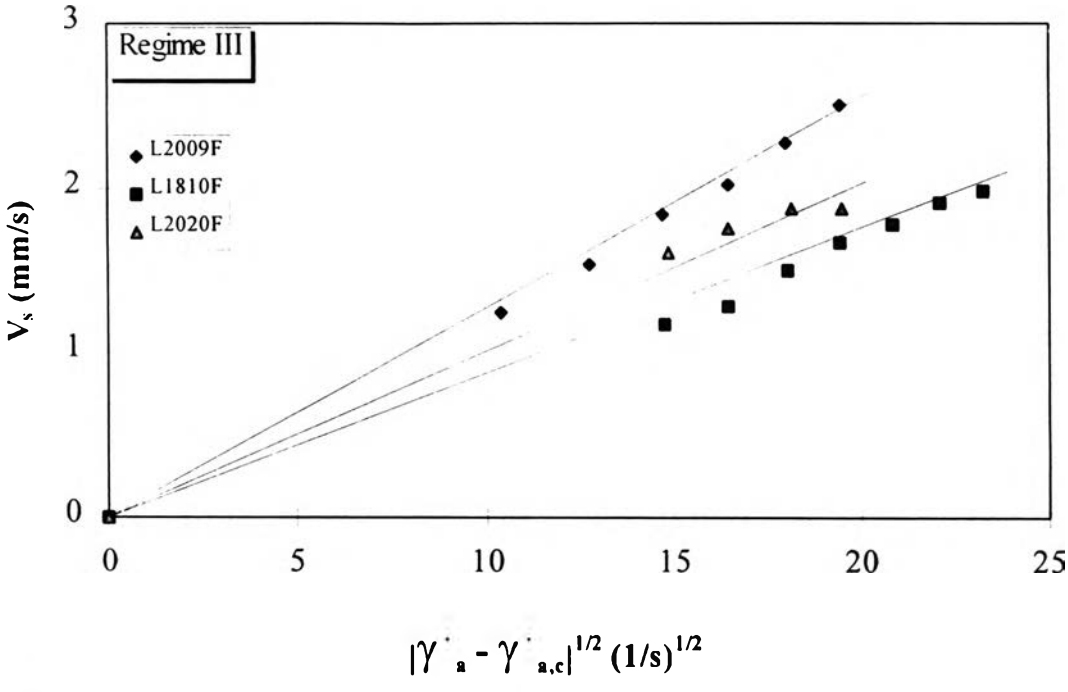

Figure 3.6(a) Slip velocity vs. $|\dot{\gamma}_a - \dot{\gamma}_{a,c}|^{1/2}$ of LLDPE in regime III.

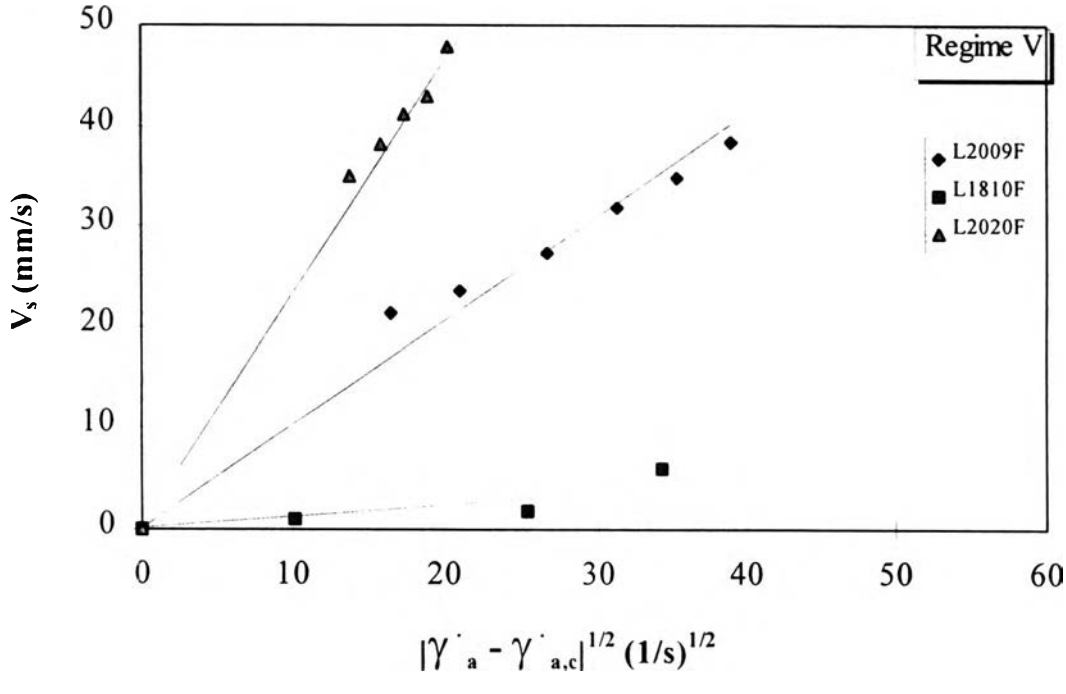

Figure 3.6(b) Slip velocity vs. $|\dot{\gamma}_a - \dot{\gamma}_{a,c}|^{1/2}$ of LLDPE in regime V.

3.4 Load and Extrudate Wavelengths

The load wavelength λ_l was determined from severals period of load oscillation using the incompressibility constraint as shown in equation 2.20. The extrudate wavelength λ_e was measured directly by a ruler with a resolution of 1 mm. They would be expected to be identical if melt was incompresible. Figures 3.7(a) and (b) show that the load wavelength seem to be dependent on strain rate in both of the oscillating regimes III and V. The experiment in each regime was carried out using a single barrel of material. It is known that λ_l is a linear function of the amount of material remaining in the barrel (Hatzikiriakos and Dealy,1992). Our result agrees with the previous finding provided that the amount of material in the barrel is more than half full. When the amount of melt in the barrel was less than half full, the reverse was seen to occur, especially in regime III. A more systematic way of looking at relationship between the extrudate wavelength and the load wavelenght is to examine the wavelenght ratio.

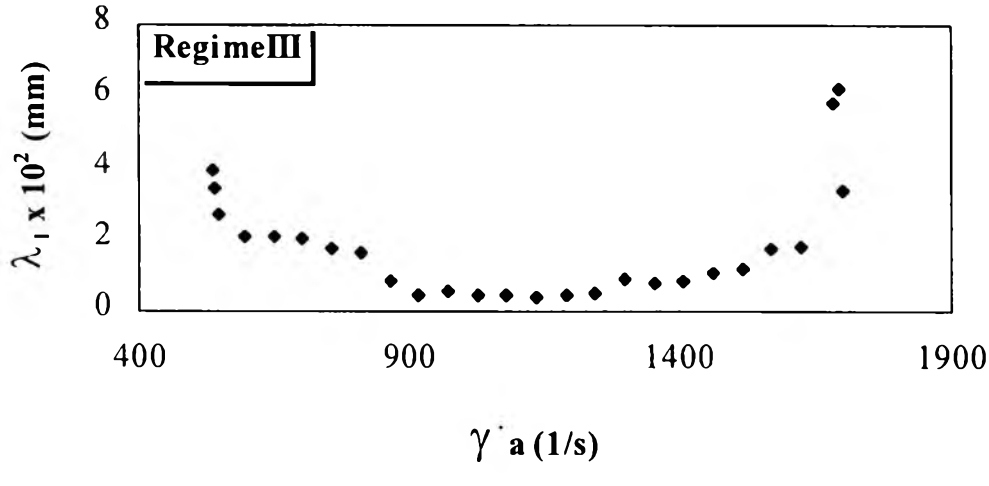

Figure 3.7(a) Wavelength vs. strain rate of LLDPE (L1810F) in regime III.

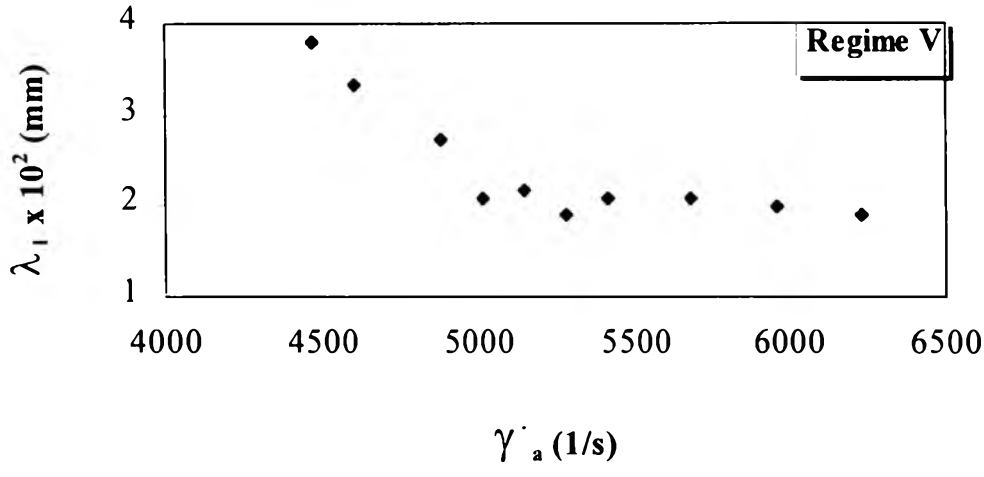

Figure 3.7(b) Wavelength vs. strain rate of LLDPE (L1810F) in regime V.

The ratio of the load wavelength (λ_l) and the extrudate wavelength (λ_e) is shown in figure 3.8. We can see that the wavelength ratio is always larger than unity. The departure from unity can be accounted for by the effect of the melt compressibility and the temperature difference between the two wavelengths measured.

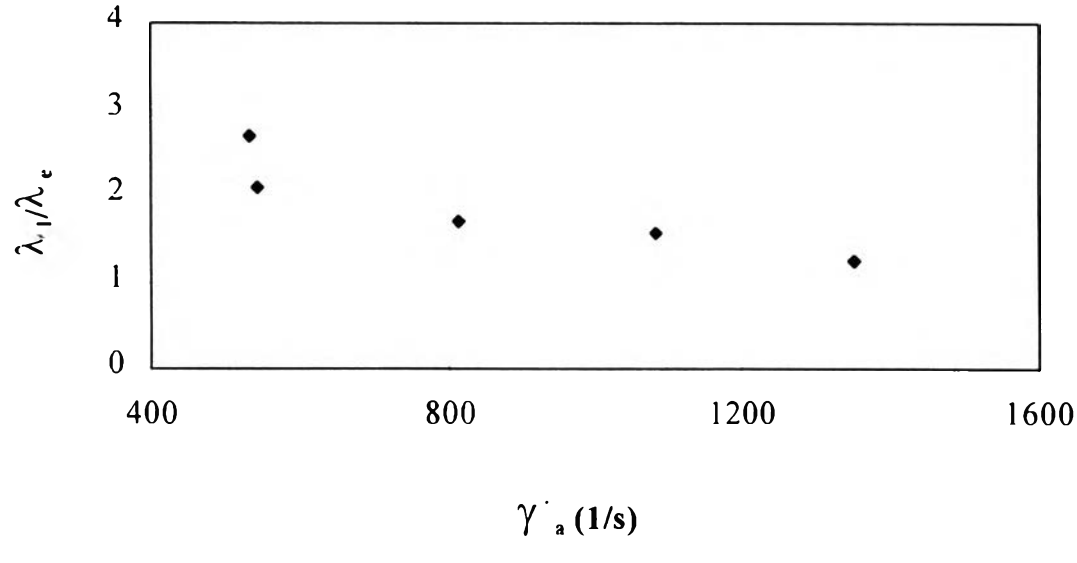

Figure 3.8 The ratio of load and extrudate wavelength vs.the apparent strain rate of LLDPE (L1810F).

3.5 Recoverable Shear

The recoverable shear is defined as

$$S_R = \frac{\tau_w}{G'}, \tag{3.1}$$

where τ_w is the wall shear stress and G' is shear modulus of the melt. Figures 3.9 (a) and (b) show the time and temperature superposition of the master curve of G' of LLDPE. In this study, we used the storage modulus (G') to represent the shear modulus and obtained the value of G' by two methods. The first method used the *asymptotic* value of G' which was obtained from the limit of G'(ω) as $\omega \rightarrow \alpha$ or G_g. Asymptotic normalization was done by setting G' in equation (3.1) equal th G_g or the glassy storage modulus:

$$S_R = \frac{\tau_w}{G_g}, \tag{3.2}$$

where G_g was determined from master curves of G' at the melt flow temperature. The master curves were obtained through measurement of G' as a function of frequency at various temperatures. Then the principle of time and temperature superposition was applied to shift G' curves at different temperatures to form a single master curve of a fixed reference temperature which was the same as the melt flow temperature. The other value was a *local* value which was obtained at the frequency (ω) corresponding to the critical strain rate of sharkskin surface. Local normalization was done by setting G' in equation (3.1) equal to G'(ω) where ω is

$$\omega = 2\pi\gamma_{a,c} \times \frac{h}{R}, \tag{3.3}$$

here ω is the angular frequency of G'(ω) obtained from the parallel plates rheometer, $\gamma_{a,c}$ is the critical apparent strain rate of the sharkskin, h is the gap spacing and R is the plate radius. The recoverable shear is shown in Table 3.6 and 3.7.

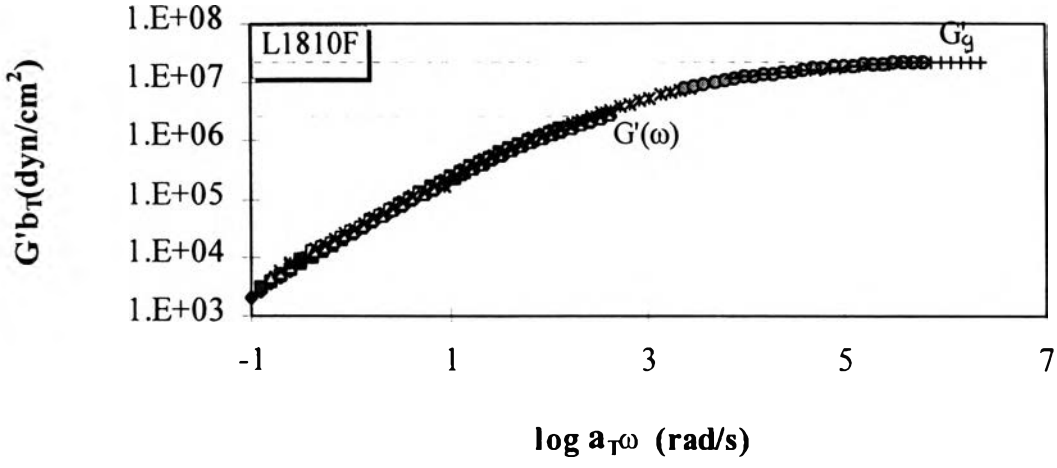

Figure 3.9(a) Master curve of G' of LLDPE(L1810F) at 185-115°C.

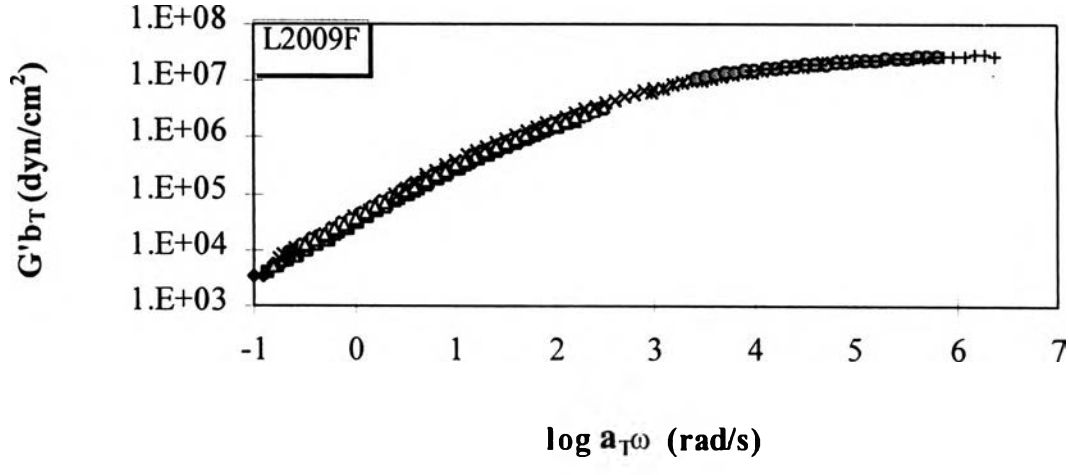

Figure 3.9(b) Master curve of G' of LLDPE(L2009F) at 185-115°C.

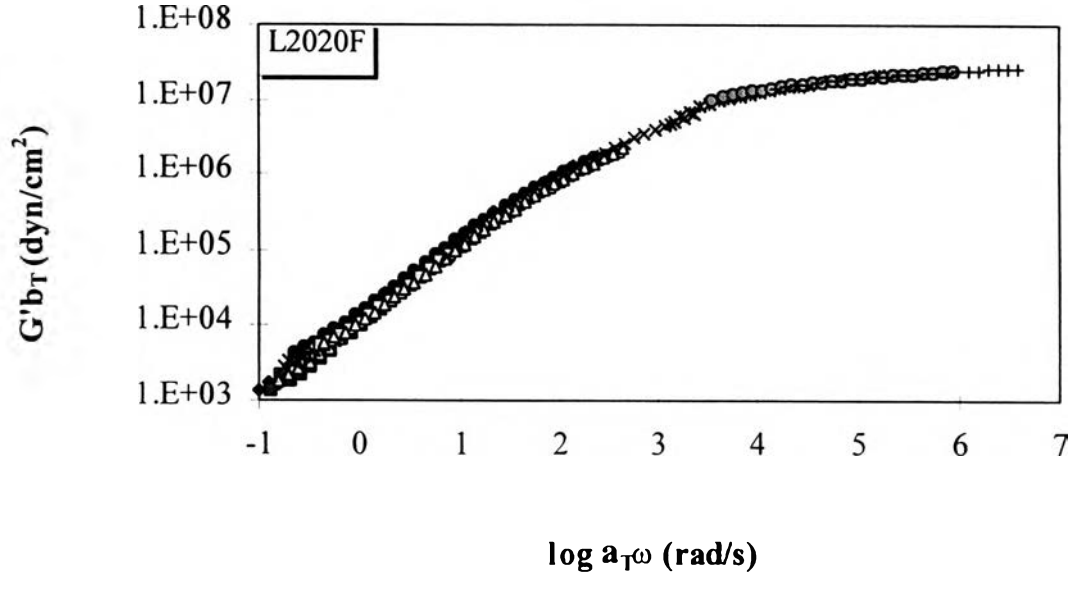

Figure 3.9(c) Master curve of G' of LLDPE(L2020F) at 185-115°C.

Table 3. 6 Recoverable shear (S_R) of sharkskin surface (regime II) of the three LLDPE's of different M_W

LLDPE	S_R(asymptotic value)	S_R(local value)
L1810F	0.1400	1.4908
L2009F	0.1449	1.5023
L2020F	0.1399	1.5525

It is interesting to note that each of the local and asymptotic S_R assumes a consistent value with respect to the material or molecular weight. The local S_R value of the sharkskin surface happens to be consistent with the S_R value of Kalika and Denn (1987) who have used the asymptotic G' values. It is possible that normalization by the asymptotic method of Kalika and Denn was inappropriate because G' was not fully measured or that G_g was not obtained directly but through extrapolation. The onset of sharkskin surface for all polymers is usually correlated with a critical value of the recoverable shear in range of 1 - 2 (Petrie and Denn, 1976). We conclude that both methods give consistent results where S_R is independent of molecular weight, and either method can be employed to characterize the onset of the sharskskin provided that the melt is throughly characterized.

Table 3.7 Asymptotic recoverable shear (S_R) of the three LLDPE's of different M_W

Regime	L1810F	L2009F	L2020F
III	0.1582	0.1621	0.1593
IV-a	0.1638	0.1714	0.1613
IV-b	0.1927	0.1868	0.1819
V	0.2138	0.2220	0.2189

It can be seen from this regime that the asymptotic recoverable shear for each regime is independent of molecular weight. However, the asymptotic recoverable shear depends on the regime or the skin texture that appears; S_R is larger for regime IV-a than regime III, for an example. Therefore, an appearance of each skin texture requires a different level of S_R to initiate a surface texture.

3.6 Stability Diagram

The stability diagram of the sharkskin defects is not available in literature, so the proposed the work is original. We are aware of stability analyses of melt capillary flow employing various constitutive models (Middleman, 1977). None of these numerical work addressed or linked flow instabilities to the extrudate skin defects. Stability diagram is defined as the separation of regimes in a parameter space; the parameters are generally normalized. So that, if all relevant parameters are accounted for, the stability diagram should be universal. We chosed λ_S/ε_S as a normalized skin parameter where λ_S is the wavelength (the length between the depth) of the sharkskin extrudate and ε_S is the amplitude (the height of the depth) of the sharkskin extrudate. A second normalized parameter is the Weissenberg number (W_i) which is defined as

$$W_i = \tau^* \times \dot{\gamma}_{a,c}, \tag{3.4}$$

where $\dot{\gamma}_{a,c}$ is the critical apparent strain rate at which sharkskin defect occurred and τ^* is the stress relaxation time scale which is calculated from

$$\tau^* = \frac{\eta_o}{G_g}. \tag{3.5}$$

Here η_o is the viscosity at zero shear rate taken from the capillary rheometer and G_g is the storage modulus in the glassy zone measured using the parallel

plate rheometer. The physical interpretation of W_i is that it is a time scale ratio of the molecular motion and the continuum flow motion. Therefore the stability diagram is two dimensional in the λ_S/ε_S vs. W_i plane. Third normalized parameter chosen was S_R, therefore another possible stability diagram is a λ_S/ε_S vs. S_R plane. Now we will describe how we obtained λ_S/ε_S and the stability diagrams.

3.6.1 Skin Parameters (λ_S, ε_S)

The characteristics of sharkskin were determined from SEM (scanning electron microscope). Figure 3.10 shows how we measured the sharkskin wavelength (λ_S) and the sharkskin amplitude (ε_S). SEM digitized the pictures of the sharkskin defect in both of the second and the third regimes by a ruler of *SemAfore* software program. The resolution of this ruler was 1/540 mm. We used the average value of at least four repeated measurements and the standard deviation over the mean value of the sharkskin wavelength (λ_S) was 1.15 and standard deviation over the mean value of the sharkskin amplitude (ε_S) was also 1.15.

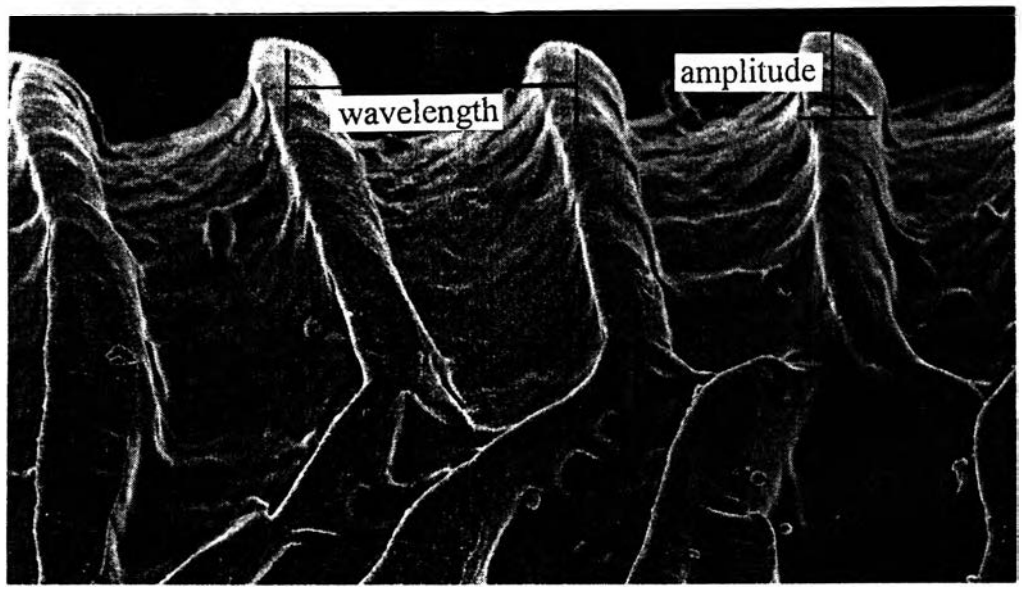

Figure 3.10 Sharkskin surface of LLDPE (L1810F) from SEM (200x magnification) and the measured wavelength (λ_S) and amplitude (ε_S) at 185°C.

Figures 3.11-3.15 show the sharkskin wavelength (λ_S) and the sharkskin amplitude (ε_S) as a function of the apparent strain rate for the three LLDPE's and the two HDPE's. Both the sharkskin wavelength (λ_S) and the sharkskin amplitude (ε_S) are linearly increasing functions of the apparent strain rate ($\dot{\gamma}_a$), for both regimes and all materials investigated with the exception of L2020F LLDPE. For this material, the molecular weight was lowest; the sharkskin wavelength (λ_S) and the sharkskin amplitude (ε_S) seem to be independent of the apparent strain rate ($\dot{\gamma}_a$).

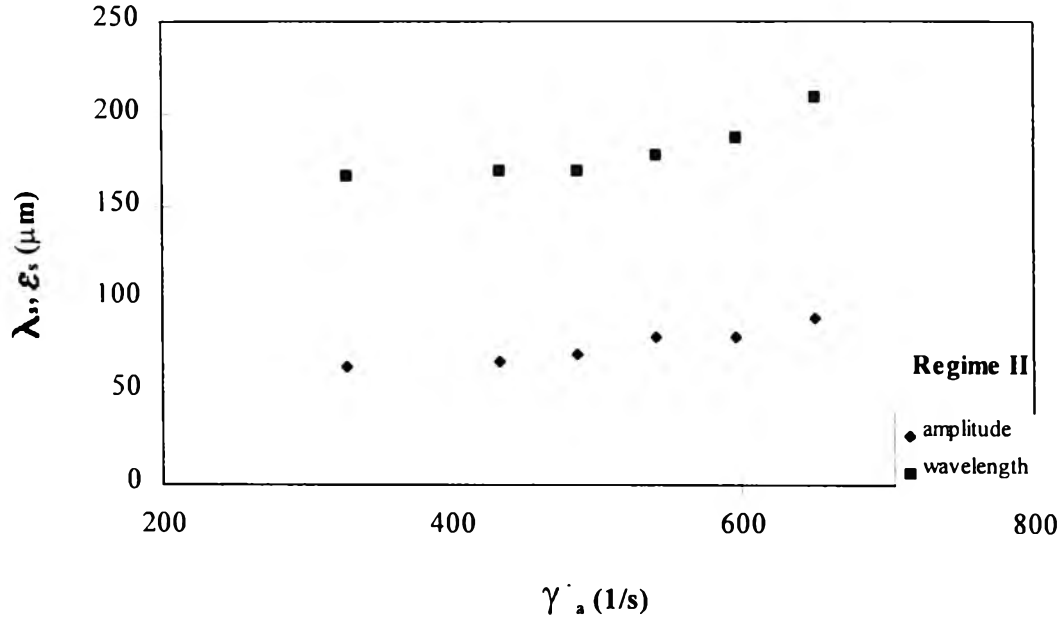

Figure 3.11(a) The wavelength (λ_S) and the amplitude (ε_S) vs. the apparent strain rate at 185°C of the sharkskin of LLDPE (L1810F) in regime II.

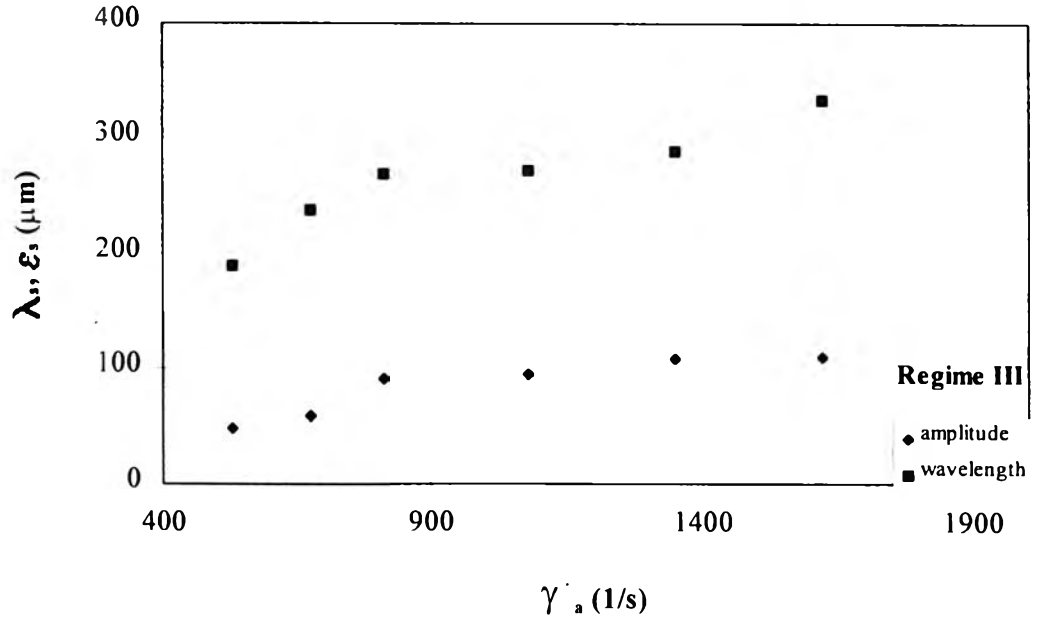

Figure 3.11(b) The wavelength (λ_S) and the amplitude (ε_S) vs. the apparent strain rate at 185°C of the sharkskin of LLDPE (L1810F) in regime III.

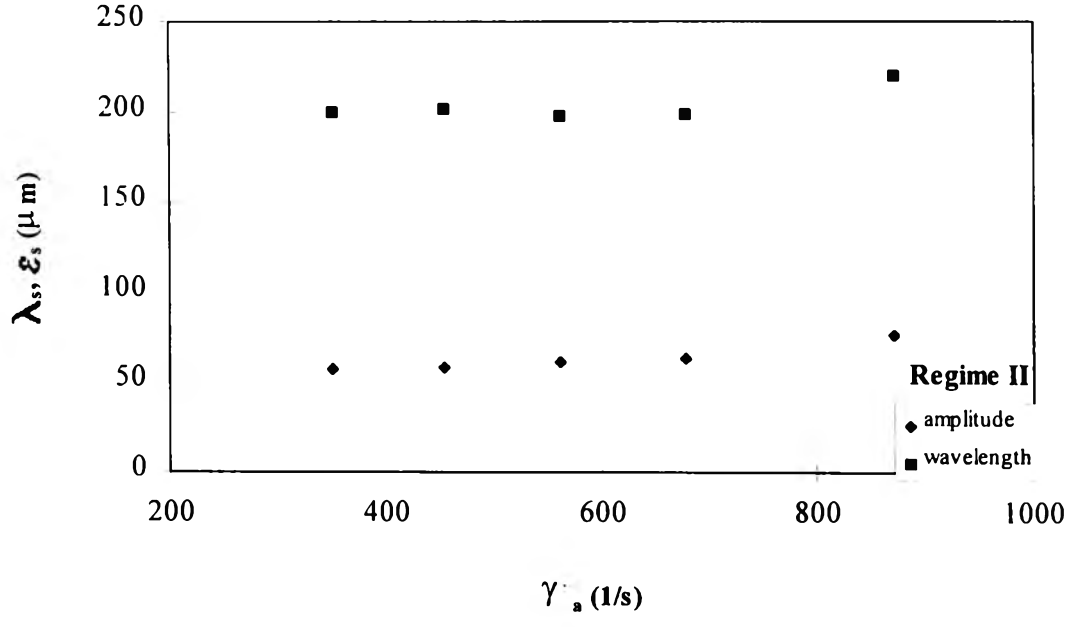

Figure 3.12(a) The wavelength (λ_S) and the amplitude (ε_S) vs. the apparent strain rate at 185°C of the sharkskin of LLDPE (L2009F) in regime II.

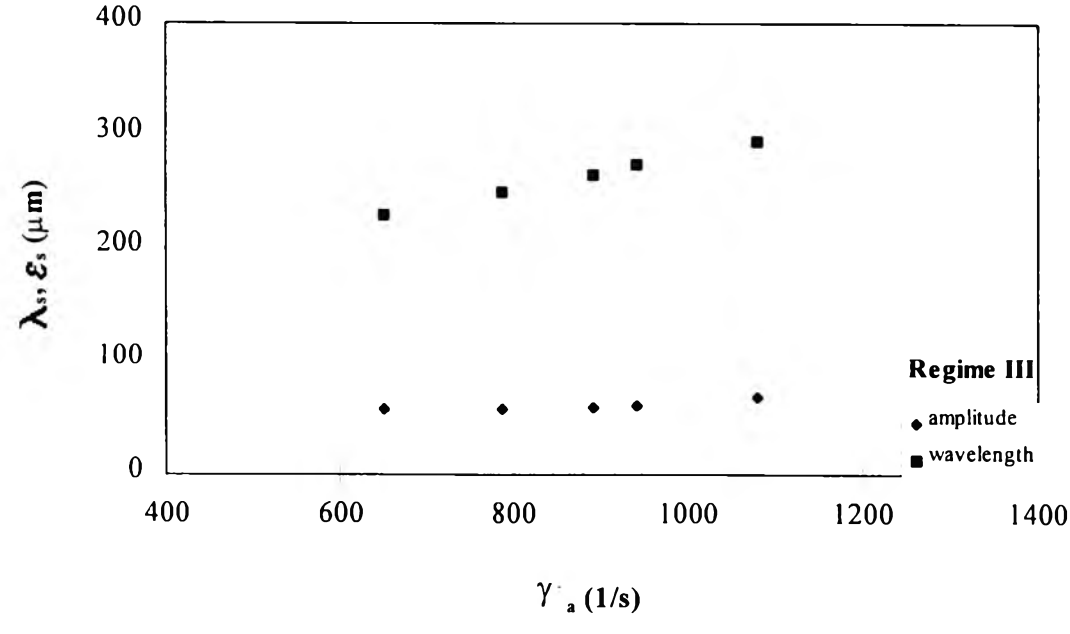

Figure 3.12(b) The wavelength (λ_S) and the amplitude (ε_S) vs. the apparent strain rate at 185°C of the sharkskin of LLDPE (L2020F) in regime III.

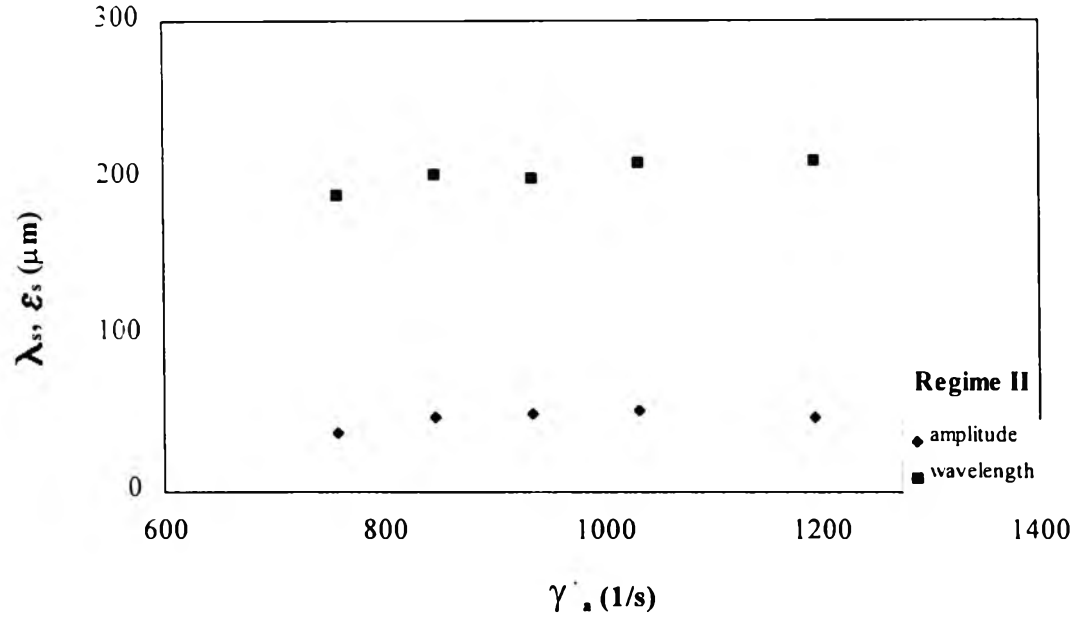

Figure 3.13(a) The wavelength (λ_S) and the amplitude (ε_S) vs. the apparent strain rate at 185°C of the sharkskin of LLDPE (L2020F) in regime II.

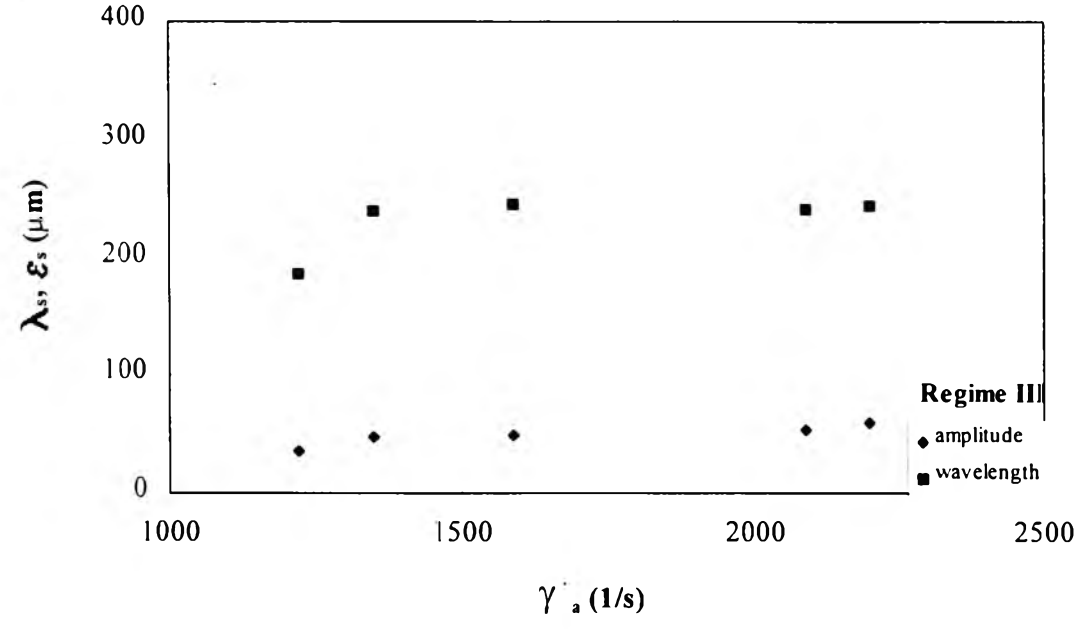

Figure 3.13(b) The wavelength (λ_S) and the amplitude (ε_S) vs. the apparent strain rate at 185°C of the sharkskin of LLDPE (L2020F) in regime III.

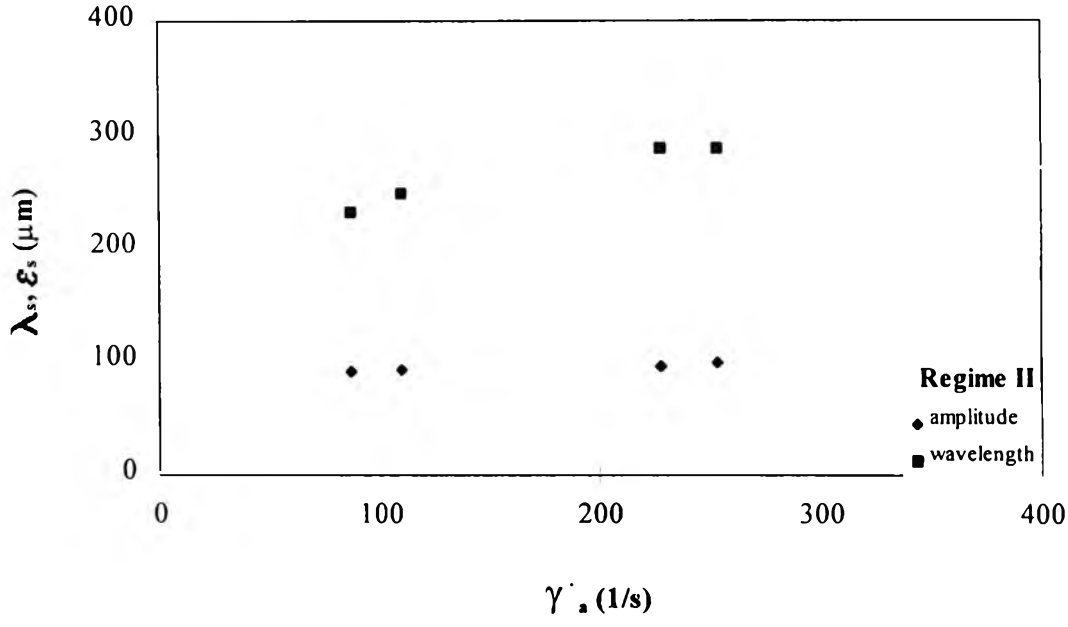

Figure 3.14(a) The wavelength (λ_S) and the amplitude (ε_S) vs. the apparent strain rate at 180°C of the sharkskin of HDPE (H5690S) in regime II.

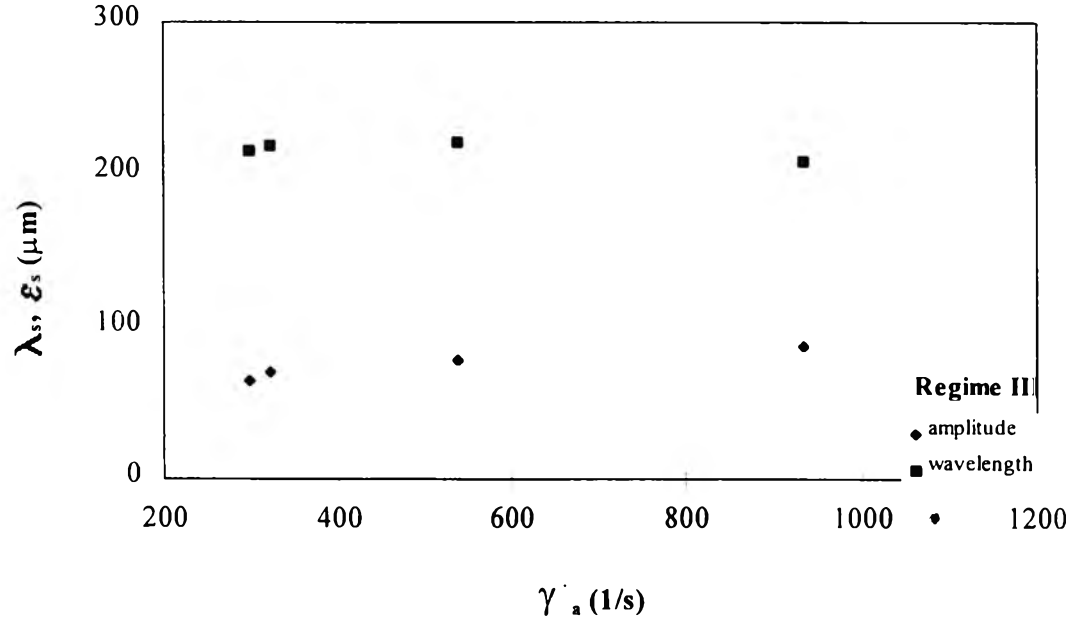

Figure 3.14(b) The wavelength (λ_S) and the amplitude (ε_S) vs. the apparent strain rate at 180°C of the sharkskin of HDPE (H5690S) in regime III.

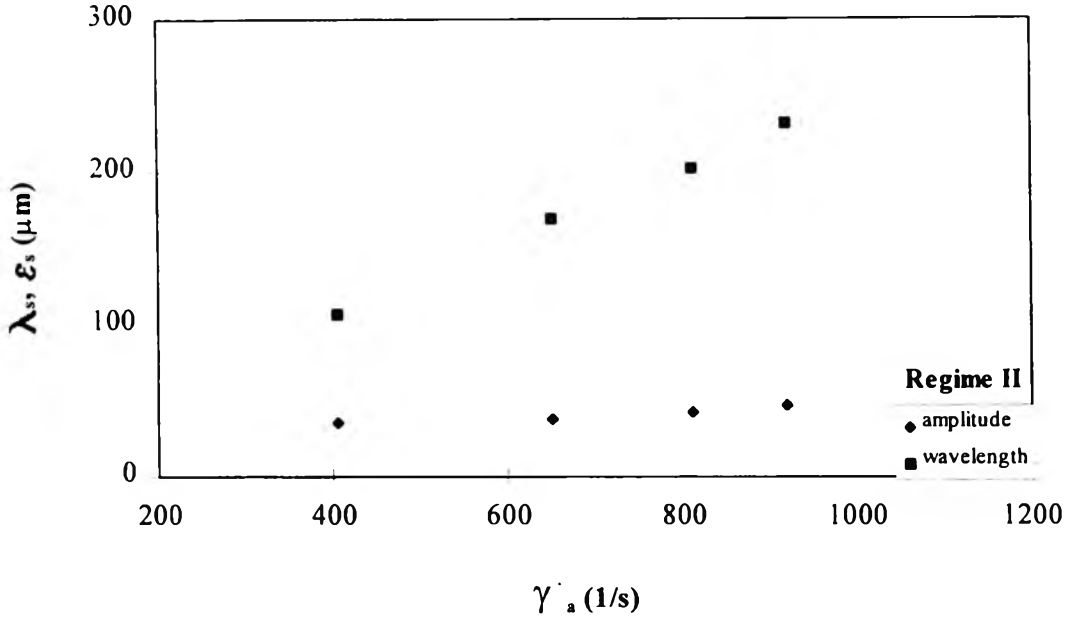

Figure 3.15(a) The wavelength (λ_S) and the amplitude (ε_S) vs. the apparent strain rate at 180°C of the sharkskin of HDPE (R1760) in regime II.

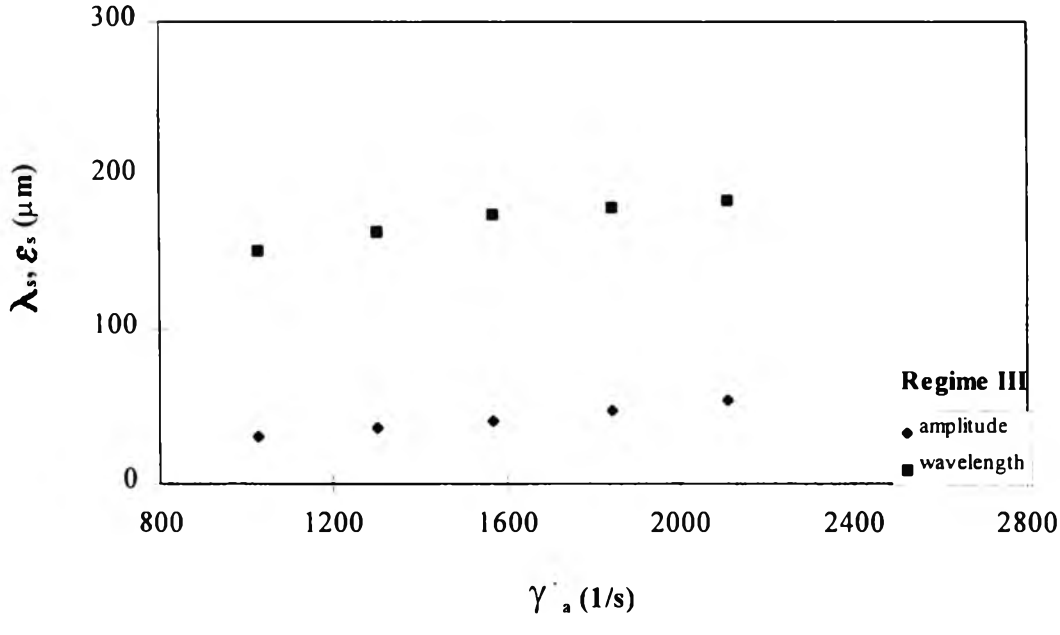

Figure 3.15(b) The wavelength (λ_S) and the amplitude (ε_S) vs. the apparent strain rate at 180°C of the sharkskin of HDPE (R1760) in regime III.

Figures 3.16 (a) and (b) show the sharkskin normalized length scale vs. the apparent strain rate ($\dot{\gamma}_a$) for all materials investigated The scatters of λ_S/ε_S vary between 2 - 5 in the range the apparent strain rate ($\dot{\gamma}_a$) investigated, so a definite conclusion cannot be drawn regarding the dependence of λ_S/ε_S or the apparent strain rate ($\dot{\gamma}_a$). But it seems possible that λ_S/ε_S is independent of the molecular weight and the structure of materials.

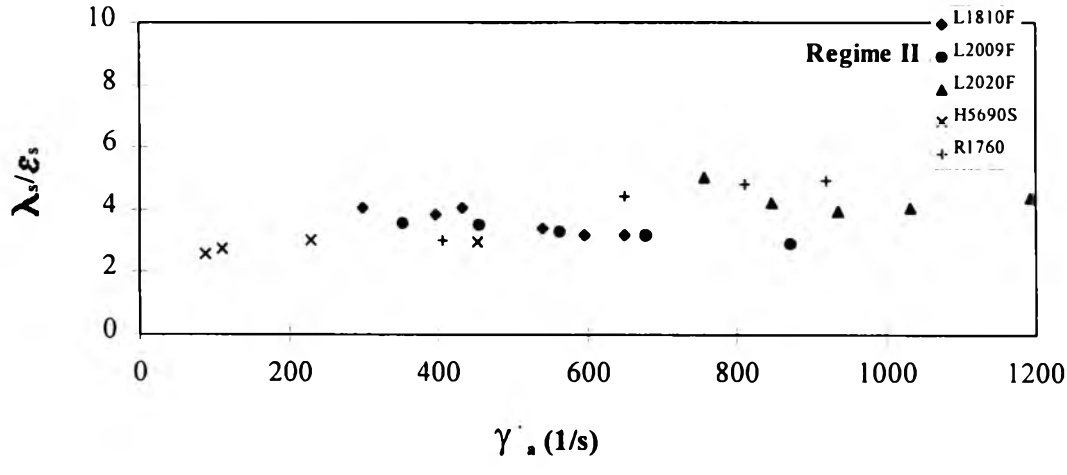

Figure 3.16(a) The sharkskin normalized length scale (λ_S/ε_S) vs. the apparent strain rate at 185°C and 180°C in regime II.

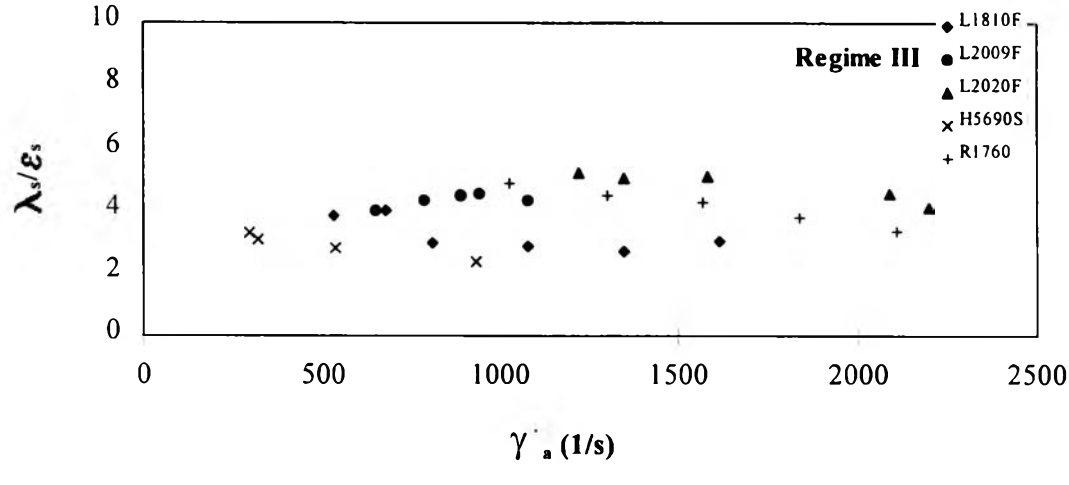

Figure 3.16(b) The sharkskin normalized length scale (λ_S/ε_S) vs. the apparent strain rate at 185°C and 180°C in regime III.

3.6.2 λ_S/ε_S vs. W_i - Stability Diagrams

Figures 3.17 (a) and (b) show the stability diagram (W_i vs. λ_S/ε_S) of the sharkskin surface for the regime II and regime III. To construct a complete stability diagram, we should have more than three points of LLDPE's, so we included the results of two HDPE's from Naiyakul (1997) and Polnark (1997). In the regime II, we see that there is a linear relation between λ_S/ε_S and W_i. This line constitutes a texture boundary between the smooth texture and the sharkskin texture for the LLDPE's. However this line is not unique as a new texture boundary can be found for the HDPE's.

In the regime III, a single texture boundary is found, separating the smooth texture and the sharkskin texture. This boundary appears to be linear in the W_i - λ_S/ε_S plane and independent of the materials investigated.

3.6.3 λ_S/ε_S vs. S_R - Stability Diagrams

Figures 3.18 (a) and (b) show the stability diagram (S_R vs. λ_S/ε_S) of the sharkskin surface for the regime II and regime III. In the regime II, there are two boundaries, one for the three LLDPE's and the other one for the two HDPE's. Therefore initial stability diagram for the sharkskin is not unique but depending on the type or the structure of the materials investigated.

In the regime III, there is only one texture boundary between the smooth texture and the sharkskin texture. This boundary is independent of the materials investigated.

We have not investigated the effects of the temperature, l_c/d_c ratio, wider range of molecular weight and the distribution. It possible that these factors are and could be very important in the sharkskin stability diagram.

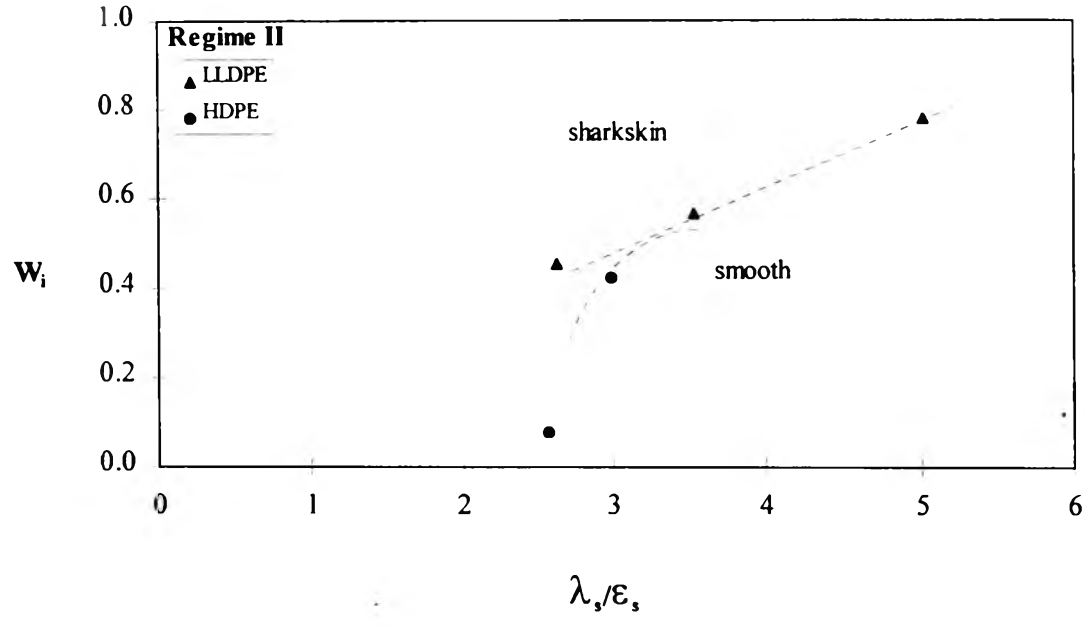

Figure 3.17(a) Stability diagrams (W_i - λ_S/ε_S) of the sharkskin surface in regime II.

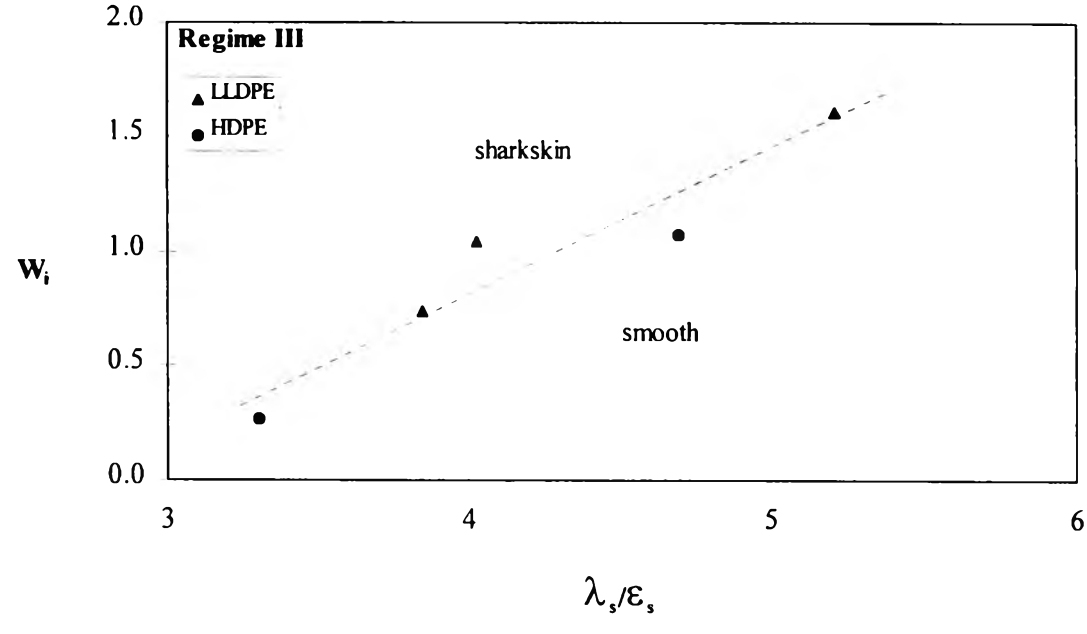

Figure 3.17(b) Stability diagrams (W_i - λ_S/ε_S) of the sharkskin surface in regime III.

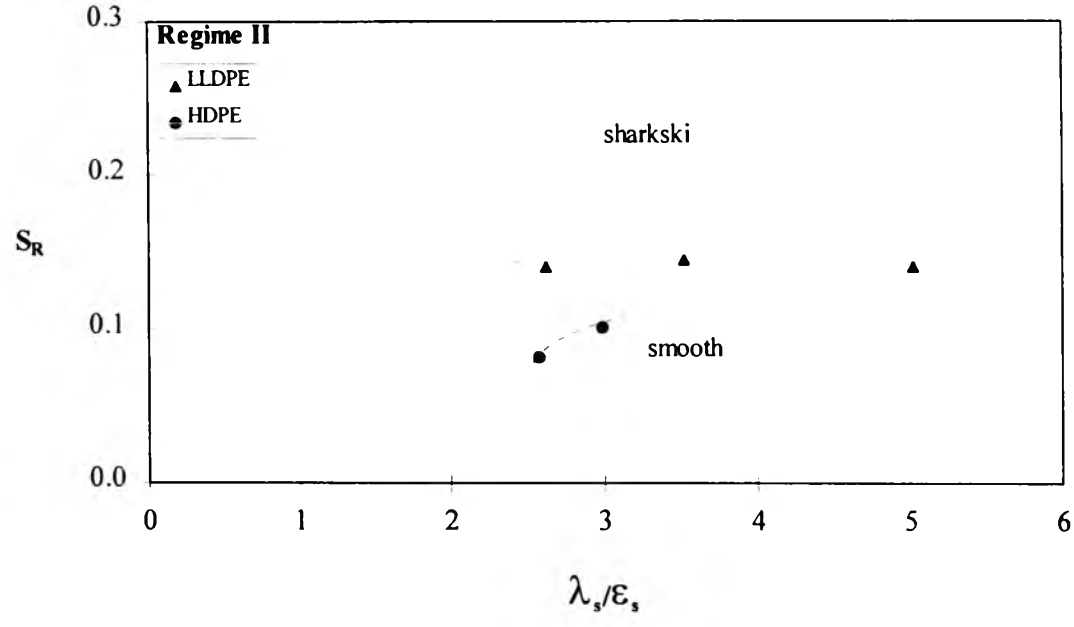

Figure 3.18(a) Stability diagrams (S_R - λ_S/ε_S) of the sharkskin surface in regime II.

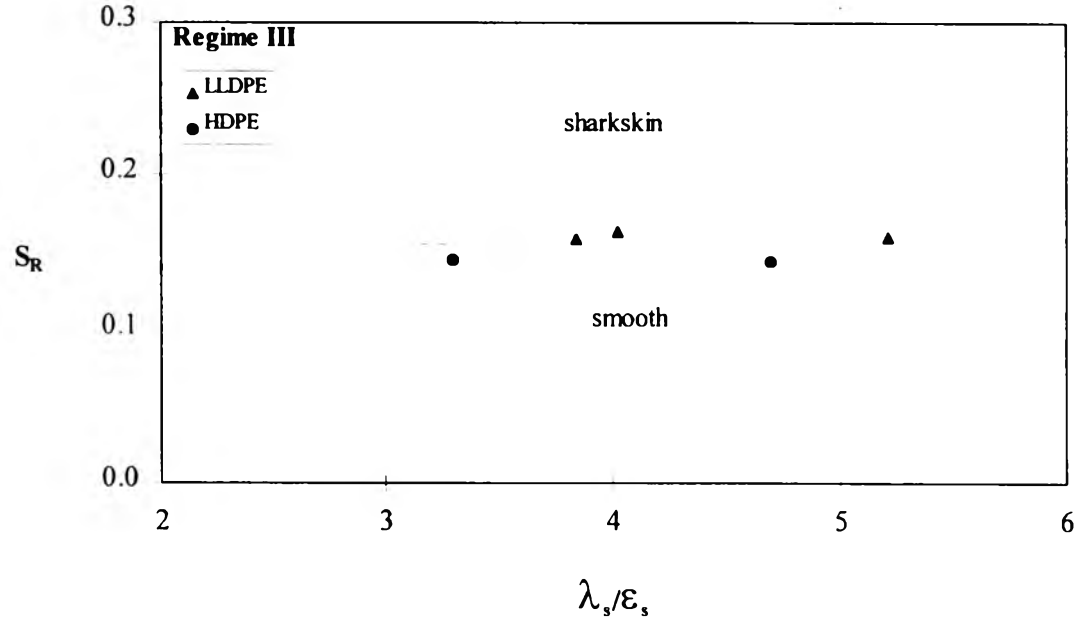

Figure 3.18(b) Stability diagrams (S_R - λ_S/ε_S) of the sharkskin surface in regime III.